


Handbook  
for  
Generic Photonic IC Design

Editors: Meint Smit and Xaveer Leijtens

4-4-2026

 *Handbook for generic photonic IC design*, by the *Photonic Integration group*, Technische Universiteit Eindhoven, is licensed under a Creative Commons “Attribution-NonCommercial-NoDerivatives 4.0 International” license.

We traced the ownership of all figures used as far as we could. However, if you are a copyright owner and believe we used your work without permission, please contact us at [coordinator@jeppix.eu](mailto:coordinator@jeppix.eu).

# Chapter 3

## Semiconductor Physics (draft)

DAAN LENSTRA, WITH CONTRIBUTIONS OF MEINT SMIT, WEIMING YAO,  
YI WANG AND JOS HAVERKORT

### List of Fundamental Constants

Quantity	Symbol	Numerical Value	Unit
Speed of light in vacuum	$c$	$2.99792458 \times 10^8$	$\text{ms}^{-1}$
Dielectric constant	$\epsilon_0$	$8.854187817 \times 10^{-12}$	$\text{Fm}^{-1}$ or $\text{AsV}^{-1}\text{m}^{-1}$
Planck constant	$h$	$6.626070041 \times 10^{-34}$	Js
$h/2\pi$	$\hbar$	$1.054571800 \times 10^{-34}$	Js
Elementary charge	$e$	$1.602176621 \times 10^{-19}$	C
Electron mass	$m$	$9.109383561 \times 10^{-31}$	kg
Rydberg constant	$R$	$1.097373157 \times 10^7$	$\text{m}^{-1}$
Boltzman constant	$k_B$	$1.380648528 \times 10^{-23}$	$\text{JK}^{-1}$

### 3.1 Introduction

It is the aim of this chapter to provide the physical background for understanding the operation of active waveguide devices, like optical amplifiers, detectors, modulators and saturable absorbers. The explanation is focused on the properties of a short active waveguide section built from semiconductor material, as depicted in Figure 3.1, which we consider as a basic cell in longer building blocks which can be analysed as

---

This chapter is heavily inspired by and based on Semiconductor Physics and Devices, Basic Principles, by Donald A. Neamen; Master Course Photonics (Ghent University) by Roel Baets and Günther Roelkens; Fundamentals of Semiconductor Lasers by Takahiro Numai; Electronic and Optoelectronic Properties of Semiconductor Structures, by Jasprit Singh; SOLID STATE PHYSICS PART II: Optical Properties of Solids by S. Dresselhaus; Fundamentals of Semiconductors, by Yu and Cardona; Physics of Semiconductor Devices, by Sze, Li and Ng; Thermal Physics, by C. Kittel and H. Kroemer

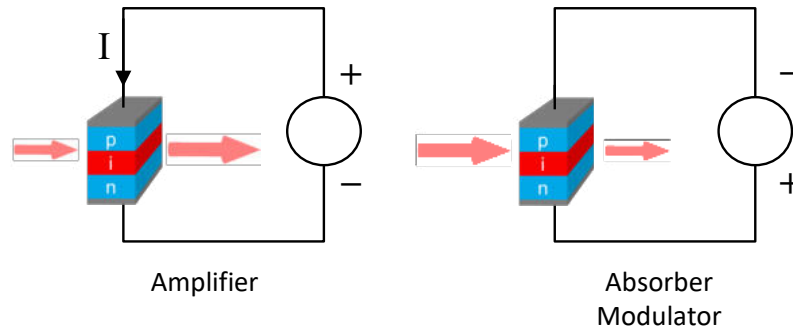


**Figure 3.1:** Basic Semiconductor Optical Amplifier cell, which works as an absorber, an optical detector or a modulator when reverse biased

concatenations of basic cells. The most important building block which can be considered as a concatenation of forward biased basic cells is the Semiconductor Optical Amplifier. Detectors, Phase modulators, and (Saturable) Absorbers can be considered as concatenations of reverse biased basic cells. The description of these building blocks is given in parts II and III of the book. In this chapter the properties of semiconductors and the basic cells in which they are applied are discussed: their band structure, the effect of doping on the semiconductor properties, pn- and pin-junctions, Double Hetero-structures, Quantum Wells, light absorption, emission and amplification. The electro-optical effects which are relevant in modulators are described in Chapter 17.

## 3.2 Semiconductor crystal structure

### 3.2.1 Crystal structure.

Modern photonic and micro-electronic components and circuits are based on semiconductor materials. The most well-known semiconductor is silicon, it is the basic material for microelectronics. Silicon is tetravalent, it has four electrons in the outer electron shell. As the outer shell has room for eight electrons, it can share electrons with four other silicon atoms in order to fill the outer shell with eight electrons. The basic structure of silicon is, therefore, a tetrahedral structure as shown in Fig. 3.2, in which each silicon atom is in the center of a tetrahedron with four other silicon atoms at the corners. The crystal structure is such, that each other silicon atom is also in the center of another tetrahedron.

Silicon has excellent properties for the fabrication of electronic components and circuits. It also supports some opto-electronic functions, such as light detection and modulation, but it is not suitable for efficient generation of light, e.g. in lasers and optical amplifiers. For these functions so-called III-V compound semiconductors, such as GaAs, InP and their related materials, are much better suited. Their structure is very similar to the structure of silicon. Whereas silicon is a so-called group-IV material (it is in the IV-th column of the periodic system), III-V compound semiconductors are composed of elements from the group-III column (In or Ga) and the group-V column (As and P), in such a way that each group-III atom is surrounded by four group-V atoms, and the other way around, as depicted in Fig. 3.2. In this structure each group-III atom shares its three electrons with the five electrons of the adjacent group-V atoms, so that together they fill the outer shell with eight electrons, just like silicon. The electronic

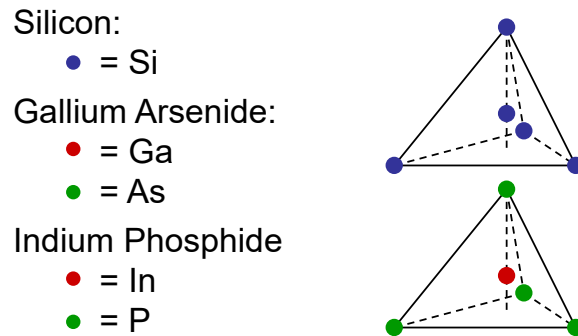


**Figure 3.2:** Basic structure of elemental and compound semiconductors.

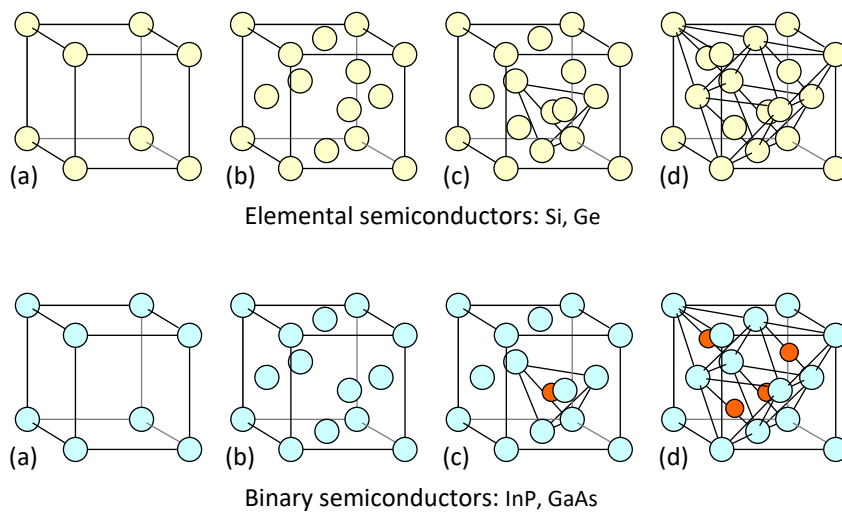


**Figure 3.3:** Structure of the cubic unit cell in a Zinc Blende crystal structure, for elemental (Si, Ge) and Binary semiconductors (InP, GaAs). The pictures labeled (d) show the full structure, the pictures labeled (a), (b) and (c) clarify how it is composed, as explained in the text.

properties of the compound semiconductors are, therefore, similar to those of silicon, although most of them support higher operation speeds than silicon. The main difference is in the optical properties, where they are used for fabrication of high-quality lasers, modulators and optical amplifiers.

The tetrahedral structure shown in Fig. 3.2 is part of the unit cell of semiconductor crystals, the unit cell is more complicated, however. The unit cell of a crystal is the smallest cell from which the crystal can be built by periodic repetition in all three directions. *unit cell*

Figure 3.3(d) shows the unit cells of silicon and compound semiconductor crystals. The cell is cubic, which means that its dimension, which is called the lattice constant, is the same in all three directions. And further it means that the faces of the unit cell are orthogonal to each other. It is a fairly complex picture, which can be understood better if we build it step by step. In Fig. 3.3(a) we see that the cell has eight atoms at the corners of the cube. Further, it has six atoms at the center of each of the six faces, as shown in Fig. 3.3(b). Fig. 3.3(c) shows how three of the face-centered atoms, *cubic crystal*

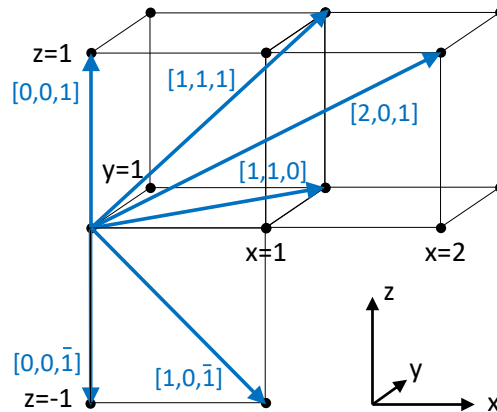


Figure 3.4: Miller indices for crystal directions.

together with one corner atom, form a tetrahedron, which has one atom in its center. For a binary semiconductor the latter is from the other group. Figure 3.3(d) shows that the unit cell contains four of these tetrahedrons, each of them with one atom in its center. This can best be seen for the binary semiconductors where the central atom has a different color. For the elemental semiconductors Si and Ge the structure is the same, however.

From the lower Fig. 3.3(d) it may seem that the unit cell contains much more atoms from one group than from the other. This is not correct, however. As we see, there are four atoms of one group fully inside the cell. For the other group there are six atoms in the center of the faces, each of which counts half because it is shared with the adjacent cell, and eight atoms at the corners, which count only for 1/8, because they are shared with seven other cells. So, together also four atoms.

*Zinc Blende* The cubic crystal structure with four tetrahedrons inside is known as the Zinc Blende structure. The crystal structure is very important for the electronic, the optical, the chemical and the mechanical properties. Cleaving planes, for example, follow crystal planes, and wet selective etchants produce side walls, the slope of which is determined by the crystal orientation. For the electronic and photonic properties the crystal structure is even more important as will be described in the following sections.

### 3.2.2 Miller Indices

Because many properties of the the semiconductor are dependent on the crystal orientation it is important to have a good description of crystal directions and crystal planes. Such a description is provided by the so-called Miller indices. We will briefly describe them here for materials with a cubic unit cell, such as silicon and the III-V compound semiconductors.

*lattice constant* **Crystal directions.** The length of the ribs of the unit cell is called the lattice constant of the crystal. For cubic crystals the lattice constant is equal in the x, y and z-direction. For InP the lattice constant is 5.8687 Å. For the definition of the Miller indices the ribs of the unit cube are normalized. The Miller indices of a crystal direction are the coordinates of the direction vectors in the normalized crystal space, as indicated in Fig. 3.4. The Miller indices of crystal directions are enclosed between square brackets [], as opposed to the coordinates of crystal planes, which are enclosed between curved

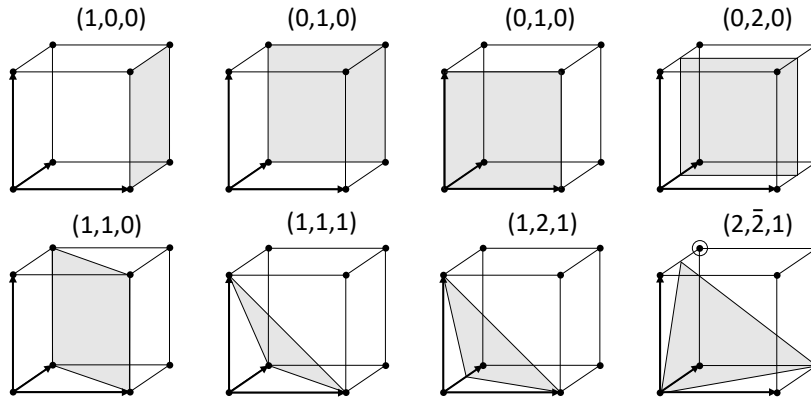


Figure 3.5: Miller indices for crystal planes.

**Problem 3.1:** Calculation of the Miller index.

**Problem:** Show that the shaded plane in the lower right unit cell of Figure 3.5 is the  $(2, \bar{2}, 1)$  plane.

**Solution:** The shaded plane intersects the  $x$ -axis and the  $y$ -axis at  $x = y = 0$  and the  $z$ -axis at  $z = 2$ . If we put a second unit cell on top of the first one, as shown in Fig. 3.6 we can extend the plane into that cell by extending the left side of the shaded triangle to the point  $(0, 1, 2)$  and going from there back to the point  $(1, 1, 0)$ . We see that in this cell the plane intersects the  $x$ ,  $y$  and  $z$ -axis at non-zero values. If we take the point  $(0, 1, 1)$  as the origin of a new coordinate system, we see that in this system the plane intersects the  $x$ -axis at  $x = 1/2$ , the  $y$ -axis at  $y = -1/2$  and the  $z$ -axis at  $z = 1$ . So the reciprocal coordinates of the plane are  $(2, \bar{2}, 1)$ .

brackets  $()$ . In the literature we see that the brackets are often omitted, so the  $(1, 1, 1)$ -plane is simply denoted as  $111$ -plane.

Fig. 3.4 shows examples for some crystal directions. The Miller indices of the  $x$ -axis are  $[1, 0, 0]$  and of the  $z$ -axis  $[0, 0, 1]$ .  $[1, 1, 0]$  is the diagonal of the two-dimensional  $xy$ -plane.  $[1, 1, 1]$  is the spatial diagonal of the three-dimensional unit cell.  $[2, 0, 1]$  is the direction in the  $x, z$  plane going through the point  $(x=2, z=1)$ . Negative directions are indicated with a small bar on top of the coordinate. So  $[1, 0, \bar{1}]$  is the planar diagonal of the lower (south-east) quadrant of the  $x$ - $z$  plane. In a cubic crystal it is perpendicular to the  $[1, 0, 1]$  direction.

**Crystal planes** Crystal planes are indicated with curved brackets  $()$  around the reciprocal coordinates of their intersections with the  $x$ ,  $y$  and  $z$ -axis. A few examples are given in Fig. 3.5. The  $x$ ,  $y$  and  $z$ -axis are indicated with bold arrows. The  $(1, 0, 0)$  plane is the shaded plane, intersecting the  $x$ ,  $y$  and  $z$ -axis at  $x = 1$ ,  $y = \infty$ ,  $z = \infty$ , so the reciprocal coordinates are  $(1, 0, 0)$ . In the same way the  $(0, 1, 0)$  plane is the  $x, z$  plane intersecting the  $y$ -axis at  $y = 1$ . Because of the periodicity of the crystal structure, the  $(0, 1, 0)$  back face ( $y = 1$ ) and the  $(0, 1, 0)$  front face ( $y = 0$ ) of the unit cell are identical. A plane halfway the  $(0, 1, 0)$  faces of the cube is the  $(0, 2, 0)$  plane. It intersects the  $y$ -axis at  $y = 1/2$ , so its reciprocal Miller index is 2.

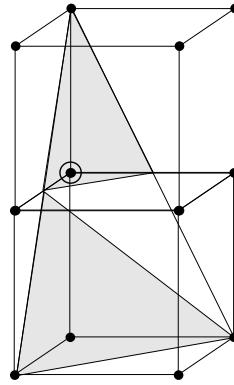


**Figure 3.6:** Configuration of the  $(2, \bar{2}, 1)$ -plane

Planes orthogonal to the axes have only one non-zero Miller index. Rotated or tilted planes have more non-zero indices. The  $(1, 1, 0)$  plane intersects the  $x$  and  $y$ -axis at  $x = y = 1$  and it is parallel to the  $z$ -axis. This plane is the natural cleaving plane of InP crystals. The  $(1, 1, 1)$  plane intersects the axes at  $x = y = z = 1$ . The  $(1, 2, 1)$  plane intersects the  $x$  and  $z$ -axis at  $x = z = 1$  and the  $y$ -axis at  $y = 1/2$ . If the plane intersects an axis in its negative range, the reciprocal Miller index is provided with a bar, e.g.  $\bar{2}$ .

For the definition of the Miller indices of a plane it is important that the plane does not go through the origin of the cell, as shown in Figure 3.5, because this would yield a reciprocal Miller index  $\infty$ . For such planes we have to find which corner of the unit cell can be used as origin of a coordinate system in which the plane intersects all three axes at non-zero values between  $-1$  and  $1$ . For the plane in the lower right figure this is the encircled corner point. In Problem 3.1 it is shown how the Miller indices of this plane can be found.

### 3.2.3 Compound semiconductors

Silicon and Germanium are so-called elemental semiconductors. Their elemental crystals consist for 100% of silicon or germanium atoms and, as shown in Fig. 3.3 they are organized in a so-called Zinc Blende structure. A similar structure can also be formed by a combination of group-III and group-V materials, or group-II and group-VI materials. Figure 3.7 shows the most commonly used materials in III-V and II-VI semiconductors. In its simplest form such a III-V semiconductor consists of two materials in a 50/50 ratio, for example In and P. We can make more complex materials with different properties, however, by replacing part of the In atoms by Ga atoms, as described in Chapter 4, Sec. 4.7. In this way a so-called ternary semiconductor is formed: InGaAs.

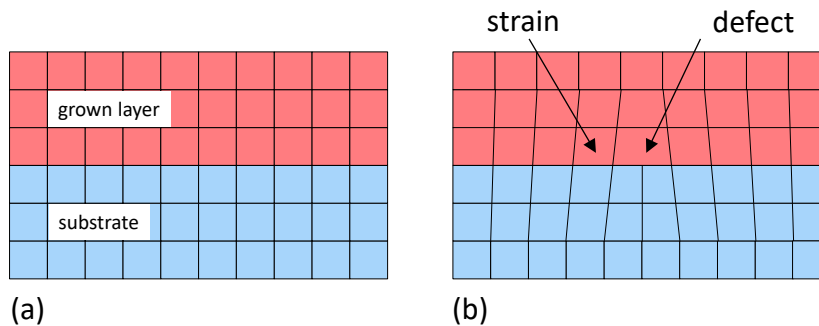
**Lattice match.** Changing the composition of the semiconductor will change its properties, e.g., the bandgap and the corresponding emission and absorption wavelength. But also properties like the refractive index. We are not free, however, to change the ratio of In and Ga at will, because the Ga atom is significantly smaller than the In atom, so that the lattice constant will shrink when we add more Ga. This is called lattice mismatch. It will cause strain when the layers are epitaxially grown, as shown in Fig. 3.8(b). Epitaxy refers to a type of crystal growth where one layer of crystalline material is deposited on a substrate, which is itself a crystal. This process ensures that the

Elemental semiconductors:	Si, Ge				
Binary semiconductors:	GaAs, InP, ... (III-V)				
Ternary semiconductors:	$In_{1-x}Ga_xAs$ (III-V)				
Quaternary semiconductor	$In_{1-x}Ga_xAs_yP_{1-y}$				

		III	IV	V	VI
		B	C	N	O
	II	Al	Si	P	S
	Zn	Ga	Ge	As	Se
	Cd	In	Sn	Sb	Te

**Figure 3.7:** Relevant part of the periodic system for the formation of elemental, III-V and II-VI semiconductors.



**Figure 3.8:** Illustration of lattice mismatch leading to strain and defects.

new layer follows the crystallographic orientation of the underlying substrate, resulting in a high-quality crystalline structure. The left figure shows the ideal case in which the lattice constant of the grown material matches that of the substrate. If it is different, however, the epitaxially grown layer will be strained and if the strain becomes too large the grown material will adapt to its own intrinsic lattice constant, which will cause defects at the interface layer.

The strain caused by replacing In with Ga can be reduced, however, if we replace at the same time part of the P atoms with As atoms. The latter are larger than the P atoms, so they increase the lattice constant and counter the effect of replacing In atoms by Ga atoms. If we replace the In atoms and the P atoms in a proper ratio with Ga and As, respectively, the lattice constant remains constant, which allows us to grow thick defect-free crystalline layers.

By doing this we get a so-called quaternary semiconductor, InGaAsP, and we describe its composition with the indices  $x$  and  $y$ , which are the fractions of In atoms replaced by Ga and the fraction of P atoms replaced by As, respectively, i.e.,  $In_{1-x}Ga_xAs_yP_{1-y}$ .

*defect*

*quaternary semiconductor*

**Bandgap Engineering** The bandgap is a characteristic feature of every semiconductor. It will be introduced and explained in the next section. The bandgap energy is denoted by  $E_g$  and has values in the order of an eV. In a quaternary semiconductor like  $In_{1-x}Ga_xAs_yP_{1-y}$  we have two degrees of freedom for varying the material properties, we can choose both  $x$  and  $y$ . In order to keep the lattice constant equal to that of the InP substrate, we have to sacrifice one degree of freedom because this requires a fixed ratio of  $x$  and  $y$ . Then we are still left with one degree of freedom, with which we can vary the emission wavelength of the semiconductor and also other properties.

Fig. 3.9 shows how the composition is related with the band gap of the compound

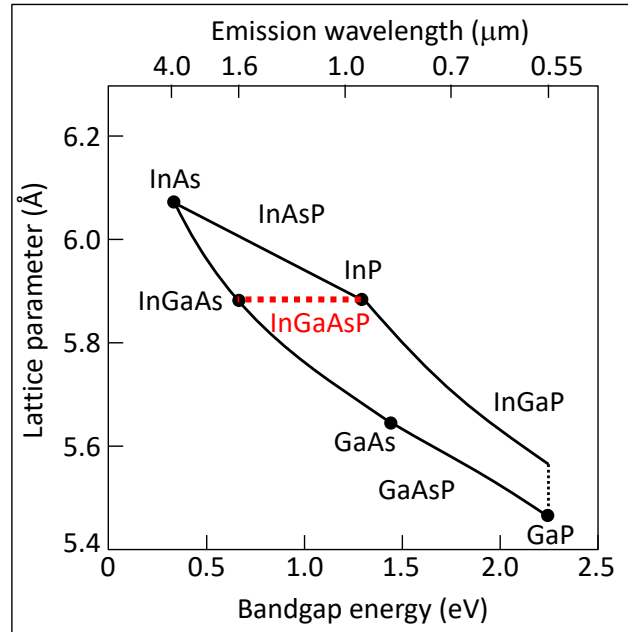


**Figure 3.9:** Bandgap vs. lattice constant diagram for III-V semiconductors.

semiconductor. The dots in the graph indicate the combination of bandgap and lattice constant for a few binary semiconductors. The lines between the dots indicate how the bandgap and the lattice constant change if we mix the two binary materials. For example, if we replace a fraction  $y$  of the P atoms in InP by As atoms, we move from the dot InP ( $y=0$ ) to the dot InAs ( $y=1$ ) via the line describing the bandgap and lattice constant of ternary  $\text{InAs}_y\text{P}_{1-y}$  material. From InAs ( $x=0$ ) we can move to GaAs ( $x=1$ ) by replacing a fraction  $x$  of the In by Ga, which will give us ternary  $\text{In}_{1-x}\text{Ga}_x\text{As}$  material. Now we see that by controlling the ratio of  $x$  and  $y$  we can move from InP ( $y=0$ ) to InGaAs ( $y=1$ ) along a horizontal line, which means that the lattice constant is the same everywhere along this line which describes the quaternary semiconductor  $\text{In}_{1-x}\text{Ga}_x\text{As}_y\text{P}_{1-y}$ . From the graph we see that by varying  $y$  between 0 and 1 we can change the emission wavelength (the wavelength corresponding to the band gap) from 0.92 eV to 1.65 eV, which covers the full C-band and O-band windows for optical communication.

*bandgap  
engineering*

We call this approach to vary the properties of ternary and quaternary semiconductors by controlling the composition during epitaxial growth *bandgap engineering*. It is widely used for InGaAsP, but it can also be used for other compound semiconductors. More information about bandgap engineering is provided in Section 4.7 of Chapter 4.

### 3.3 Band structure, Schrödinger equation and Fermi-Dirac distribution

*wave function*

Emission and absorption of light as well as electrical properties of semiconductors have a close relation to the electron energies, which in semiconductors are characterized by band structures. In a semiconductor crystal each electron is represented by a quantum mechanical wave function of the form

$$\psi_{n,k}(\mathbf{r}) = e^{i\mathbf{k}\cdot\mathbf{r}} u_{n,k}(\mathbf{r}), \quad (3.1)$$

where  $u_{n,\mathbf{k}}$  is a function with the same periodicity  $\mathbf{R}$  as the crystal, or

$$u_{n,\mathbf{k}}(\mathbf{r}) = u_{n,\mathbf{k}}(\mathbf{r} + \mathbf{R}), \quad (3.2)$$

with  $\mathbf{R}$  a vector indicating the periodicity of the crystal. In Eqs. (3.1) and (3.2),  $n$  is the band index, it labels the orbitals of the electrons around the atoms or molecules in the crystal. Because in the crystal the outer orbits of individual atoms are strongly coupled they split up in a large number of energy levels or states. Each quantum mechanical state is labeled by the combination  $(n, \mathbf{k})$  and can be occupied by two electrons, one with spin up, the other with spin down (Pauli principle). Because of the exclusion principle, the next two electrons must have a different wave vector  $\mathbf{k}$ . In fact, the wave vector  $\mathbf{k}$  is quantized, with one vector per  $(2\pi)^3/V_c$  volume in  $\mathbf{k}$ -space (reciprocal space), where  $V_c$  is the crystal volume. Hence, the density of states in  $\mathbf{k}$ -space is  $V_c/(2\pi)^3$ , but for a “macroscopically” large crystal of  $1\text{ mm}^3$ , say, the wave vector  $\mathbf{k}$  can be considered for all practical purposes as continuous.

The wave function (3.1) satisfies the Schrödinger equation

$$\left[ -\frac{\hbar^2}{2m}\nabla^2 + U_c(\mathbf{r}) \right] \psi_{n,\mathbf{k}}(\mathbf{r}) = E_n(\mathbf{k})\psi_{n,\mathbf{k}}(\mathbf{r}) \quad (3.3)$$

where  $U_c(\mathbf{r})$  is the (periodic) crystal potential with periodicity vector  $\mathbf{R}$ , i.e.,  $U_c(\mathbf{r}) = U_c(\mathbf{r} + \mathbf{R})$ , and the corresponding energy spectrum is denoted by  $E_n(\mathbf{k})$ ,  $m$  is the mass of the particle and the reduced Planck’s constant  $\hbar = h/2\pi$  equals Planck’s constant  $h$  divided by  $2\pi$ . A typical semiconductor band structure in one dimension is sketched in Fig. 3.10. As indicated, the bands are separated by a gap  $E_g$  of forbidden energy. No electron states are available in the gap. The occurrence of a bandgap is typical for semiconductors; its value is characteristic for the specific semiconductor, whether compound or pure. The three uppermost bands below the energy gap are the valence bands. The lowest band above the gap is the conduction band. Figure 3.10 shows only one band above the gap; in principle there can be more with higher energy, but they are less relevant generally. In case the minimum of the conduction band and the maximum of the valence band occur for the same  $\mathbf{k}$ -vector, one speaks of a *direct* semiconductor. When this is not the case the semiconductor is referred to as *indirect*. Transitions between the conduction band and the valence band (e.g., in case of absorption or emission of a photon) are much more probable for direct semiconductors than for indirect semiconductors, where a phonon is required to bridge the difference in  $\mathbf{k}$ -vector. Since optical transitions can occur only between electron states with the same  $\mathbf{k}$ -vector, direct bandgap semiconductors (like most III-V-semiconductors) have higher absorption or spontaneous emission than indirect bandgap semiconductors (like silicon and germanium), and they support stimulated emission, as opposed to indirect semiconductors.

In an ideal semiconductor at temperature  $T = 0\text{ K}$ , all states up to the valence bands are occupied by electrons and the conduction band is empty. At  $T > 0$  a fraction of electrons from the valence band will be thermally excited to the conduction band, leaving behind holes, or missing electrons, in the valence band. There may be other mechanisms leading to electrons in the conduction band, such as by doping the material with special atoms (see Section 3.4) or by absorption of light (Section 3.7.1).

The band structure and the band gap in particular are crucial in understanding electrical and optical properties of a semiconductor. For many applications this is especially true in the vicinity of  $\mathbf{k} = 0$ . This point in the reciprocal space (the  $\mathbf{k}$ -space) is called

*crystal periodicity  
band index*

*quantum state  
Pauli principle*

*Schrödinger  
equation*

*crystal potential  
energy spectrum*

*band structure  
energy gap  
valence band*

*conduction band*

*direct  
semiconductor  
indirect  
semiconductor*

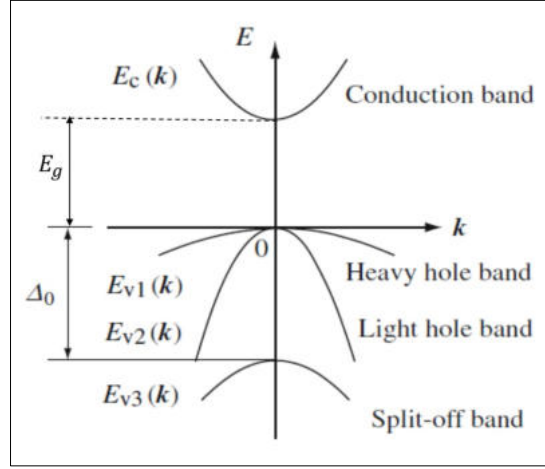


**Figure 3.10:** Typical band structure for a direct semiconductor, near  $\mathbf{k} = 0$ . There is one conduction band,  $E_c(\mathbf{k})$ , and three valence bands  $E_{\nu i}(\mathbf{k})$ , ( $i = 1, 2, 3$ ). The energy gap  $E_g$  of forbidden energy is indicated. The top of the split-off band  $E_{\nu 3}(\mathbf{k})$  lies  $\Delta_0$  below the top of the other two valence bands. This split-off energy is related to the interaction of spin and angular momentum.

*Gamma point* the  $\Gamma$ -point. It can be derived from the Schrödinger equation that important physical quantities are related to the band structure.

**Analogy between optical physics and quantum mechanics.** As the Schrodinger equation is a wave equation, there is a far reaching analogy between quantum mechanics and optical waveguide physics. If we substitute the description of a waveguide mode  $\vec{U} = U_{xy}e^{-j\beta z}$  in the Helmholtz equation  $\nabla^2 \vec{U} + k^2 \vec{U} = 0$  we obtain

$$[\nabla_{xy}^2 + n^2(x, y)k_0^2 - \beta_n^2]U_{xy} = 0$$

where  $n(x, y)$  is the refractive index profile,  $k_0$  is the wavenumber in vacuum and  $\beta_n$  is the propagation constant of the  $n$ -th mode. As we see, this formula is very similar to the Schrödinger equation

$$\left[ \nabla^2 - \frac{2m}{\hbar^2} [U_c(\mathbf{r}) - E_n(\mathbf{k})] \right] \psi_{n,\mathbf{k}}(\mathbf{r}) = 0$$

where the potential function  $\frac{2m}{\hbar^2} U_c(\mathbf{r})$  has the same role as the index profile  $n^2(x, y)k_0^2$  and the energy  $E_n(\mathbf{k})$  compares to  $\beta^2$ . In two dimensions a quantum-mechanical wave can be compared with a waveguide mode, and its energy with the (squared) propagation constant, which is also quantized; it can assume a large number of discrete values if the waveguide is strongly multimoded. So the wave functions of electrons and holes in a quantum well look very similar to the modes in a dielectric waveguide, with a cosine-like profile in the well and exponential tails in the barriers. For photonic crystals the analogy with quantum mechanics is even stronger, including forbidden bandgaps.

*electron velocity* The velocity of an electron in state  $(n, \mathbf{k})$ , for example, is given by

$$v_n(\mathbf{k}) = \frac{1}{\hbar} \nabla_{\mathbf{k}} E_n(\mathbf{k}) \quad (3.4)$$

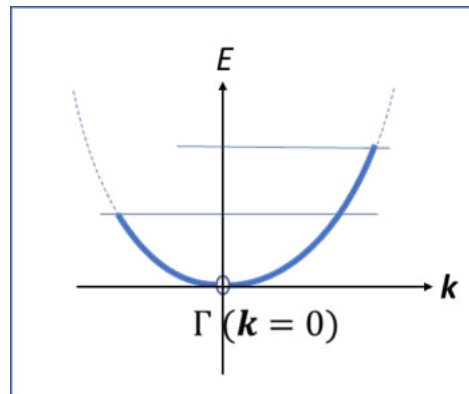


**Figure 3.11:** Example of skew band occupation representing a situation with non-zero current.

where  $\nabla_{\mathbf{k}}$  denotes the divergence in  $\mathbf{k}$ -space, with components  $\partial k_x, \partial k_y, \partial k_z$ . Note that Equation 3.4 is the quantum mechanical analogue of the group velocity of electromagnetic waves related to the dispersion relation.

*group velocity*

The effective mass  $m_n$  of the electrons and holes is related to the curvature  $\partial^2 E_n(k)/\partial k^2$  of the bands. A strong band curvature corresponds to a light mass (e.g., the light hole band in Figure 3.10), a weak curvature to a heavy mass (e.g., the heavy hole band).

*effective mass*  
*light hole band*

*heavy hole band*

The effective mass is dependent on the magnitude and the direction of the  $\mathbf{k}$ -vector and should for accurate calculations be described with a tensor. Velocity and effective mass play important roles for describing the properties of a semiconductor. For example, if  $f_n(\mathbf{k})$  denotes the probability that a state  $(n, \mathbf{k})$  is occupied by an electron, the total current density can be expressed as

$$\mathbf{j} = \frac{2e}{V_c} \sum_{n, \mathbf{k}} f_n(\mathbf{k}) \mathbf{v}_n(\mathbf{k}) \quad (3.5)$$

where the factor 2 in front is due to the spin degeneracy. By recalling the density of wave vectors in  $\mathbf{k}$ -space  $V_c/(2\pi)^3$ , we can approximate the summation over  $\mathbf{k}$  by an integration:

$$\mathbf{j} = \frac{e}{4\pi^3} \sum_n \int d^3 k f_n(\mathbf{k}) \mathbf{v}_n(\mathbf{k}). \quad (3.6)$$

In the absence of applied fields, the energy bands and their occupation probabilities are inversion symmetric, i.e., invariant for  $\mathbf{k} \rightarrow -\mathbf{k}$ . This implies that a semiconductor normally exhibits no net current, but an applied electric field can lead to a skew occupation probability and thus to a net non-zero electrical current (see Figure 3.11).

The effective mass is relevant when considering electron mobility and conductance. In thermal equilibrium, the occupation probability function, i.e. the probability that an electron occupies a quantum mechanical state with energy  $E$ , is called the Fermi-Dirac distribution, and can be derived from statistical considerations (See Kittel and Kroemer [101]). We will sketch a simplified picture for the situation at  $T = 0$  K, when the crystal is in its ground state, i.e., the state with lowest total electron energy. Each state  $(n, \mathbf{k})$  can only be occupied by two electrons at most. The lowest total energy is achieved when the lowest energy bands are occupied up to a certain maximum energy  $E_F$ , also referred to as the Fermi energy. In this case, the Fermi-Dirac distribution

*electron mobility*  
*occupation probability function*  
*Fermi-Dirac distribution*

*Fermi energy*

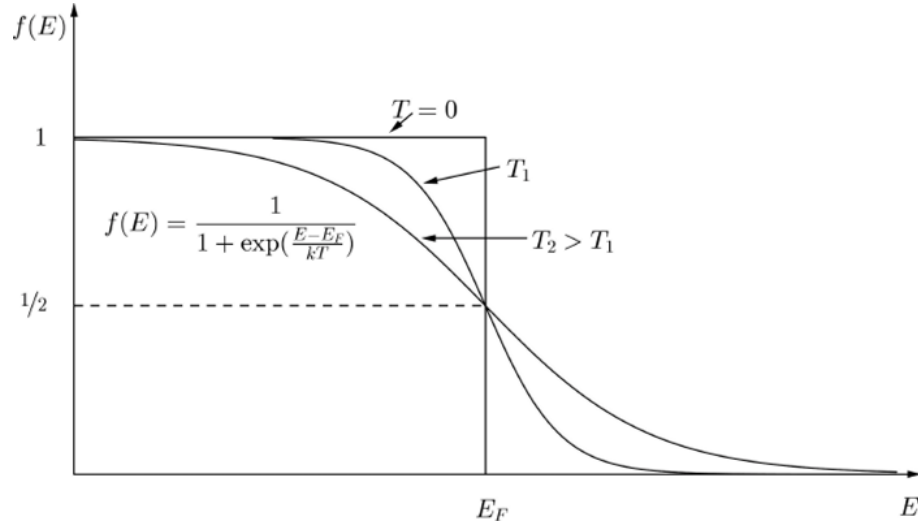


**Figure 3.12:** The Fermi-Dirac distribution function versus energy for different temperatures.

function  $f_F$  is simply given by

$$f_F(E) = \begin{cases} 1 & E < E_F \\ 0 & E > E_F \end{cases}, \quad (3.7)$$

where the value of  $E_F$  follows from the total number of electrons (see Equation 3.9). Note that Eq. 3.7 is valid only at  $T = 0$  K. For  $T > 0$ , some electrons have jumped to higher energy levels, leaving behind empty states below  $E_F$ . In that case, there is a non-zero probability that some energy states above  $E_F$  become occupied by electrons and some states below  $E_F$  will be empty.

The Fermi-Dirac distribution function for a system in equilibrium at temperature  $T$  is given by (see Kittel and Kroemer [101])

$$f_F(E) = \frac{1}{1 + \exp\left(\frac{E-E_F}{k_B T}\right)}, \quad (3.8)$$

where  $k_B$  is the Boltzmann constant. It should be noted that the Fermi energy  $E_F$  depends in principle on  $T$  because of the requirement that the total number of electrons  $N_e$  satisfies

$$N_e = 2 \sum_{n,\mathbf{k}} f_F(E_n(\mathbf{k})) \quad (3.9)$$

A plot of the Fermi-Dirac function for various temperatures is given in Figure 3.12. Note that  $f_F(E_F) = 1/2$ .

In many cases, the band structure of the conduction band can be approximated near  $\mathbf{k} = 0$  as

$$E(\mathbf{k}) = E_c + \frac{\hbar^2 \mathbf{k}^2}{2m_c}, \quad (3.10)$$

where  $E_c$  is the energy of the minimum of the conduction band and  $m_c$  is the conduction band effective mass. Similarly, the valence band energy can be approximated

as

$$E(\mathbf{k}) = E_v - \frac{\hbar^2 k^2}{2m_v}, \quad (3.11)$$

with  $E_v$  the energy of the top of the valence band and  $m_v$  the valence band effective mass. Eqns. 3.10 and 3.11 are referred to as the parabolic band approximations near  $\mathbf{k} = 0$ . In the parabolic approximation, a surface of equal energy  $E \geq E_c$  in  $\mathbf{k}$ -space is a sphere with radius  $k = \sqrt{2m_c(E - E_c)}/\hbar$  and the volume in  $\mathbf{k}$ -space of a shell with thickness  $dE$  equals  $4\pi k^2 \frac{dk}{dE} dE = 2\pi \left(\frac{2m_c}{\hbar^2}\right)^{3/2} (E - E_c)^{1/2} dE$ . When multiplied with the density of states in  $\mathbf{k}$ -space,  $V_c/(2\pi)^3$ , we arrive at the number of conduction-band states with energy between  $E$  and  $E + dE$ : *parabolic band approximation*

$$N_c(E)dE = \frac{2V_c}{(2\pi)^2} \left(\frac{2m_c}{\hbar^2}\right)^{3/2} (E - E_c)^{1/2} dE, \quad (3.12)$$

where the factor 2 in front of  $V_c$  is due to the electron spin. Then, the total density of electrons in the conduction band in equilibrium at temperature  $T$  is given by multiplying Equation 3.12 with the Fermi-Dirac function and integrating over the conduction band energy:

$$n_e = \frac{1}{V_c} \int_{E_c}^{\infty} dE N_c(E) f_F(E) = \frac{1}{2\pi^2} \left(\frac{2m_c}{\hbar^2}\right)^{3/2} \int_{E_c}^{\infty} dE \frac{(E - E_c)^{1/2}}{1 + \exp\left(\frac{E - E_F}{k_B T}\right)} \quad (3.13)$$

Here we replaced the upper value of the conduction band by  $\infty$ , which is a justified approximation because of the rapid decline of the Fermi-Dirac distribution. Moreover, if we assume that the Fermi energy lays within the gap and  $T$  is small enough that for  $E \geq E_c$ ,  $E - E_F \gg k_B T$ , we can approximate  $\frac{1}{1 + \exp\left(\frac{E - E_F}{k_B T}\right)}$  by  $\exp\left[-\frac{E - E_F}{k_B T}\right]$ , which is known

as the *Boltzmann approximation*. With this approximation Eq. 3.13 can be simplified to (see Appendix 3.13 for the derivation) *Boltzmann approximation*

$$n_e = N_c e^{-\frac{E_c - E_F}{k_B T}}, \quad (3.14)$$

where  $N_c$  is called the effective density of states in the conduction band,

$$N_c \cong \frac{1}{4} \left(\frac{2m_c k_B T}{\pi \hbar^2}\right)^{3/2}. \quad (3.15)$$

For the holes in the valence band we can follow a similar procedure. Since a hole is a non-occupied electron state, the hole equilibrium distribution is not  $f_F(E)$  but rather

$$1 - f_F(E) = \frac{1}{1 + e^{\frac{E_F - E}{k_B T}}} \approx e^{-\frac{E_F - E}{k_B T}}, \quad (3.16)$$

where the last step is again the above-introduced Boltzmann approximation, valid when  $E_F - E_v \gg k_B T$  and  $E \leq E_v$ .

In the same way as for  $n_e$  in Appendix 3A, we find for the thermal hole concentration

$$n_h = N_v e^{-\frac{E_F - E_v}{k_B T}}, \quad (3.17)$$

where  $N_v$  is called the effective density of states in the valence band,

$$N_v \cong \frac{1}{4} \left(\frac{2m_v k_B T}{\pi \hbar^2}\right)^{3/2}. \quad (3.18)$$

**Problem 3.2:** Carrier and hole concentrations in intrinsic InP and lattice-matched InGaAs.

**Problem:** Calculate at room temperature the carrier and hole concentrations in intrinsic InP and lattice-matched InGaAs.

**Solution:** At thermal equilibrium, the carrier densities are  $n_e = N_c \exp\left(-\frac{E_c - E_F}{k_B T}\right)$  and  $n_h = N_v \exp\left(-\frac{E_F - E_v}{k_B T}\right)$ . Since  $E_g = E_c - E_v$ , we can see that the product of  $n_e$  and  $n_h$  does not depend on  $E_F$ :  $n_h n_e = N_c N_v \exp\left(-\frac{E_g}{k_B T}\right)$ . For an intrinsic semiconductor with charge neutrality,  $n_e = n_h = n_i$ . Therefore,  $n_i = \sqrt{n_h n_e} = \sqrt{N_c N_v} \exp\left(-\frac{E_g}{2k_B T}\right)$ . [102]. Assume  $T = 300$  K, then

1. InP:  $E_g \approx 1.344$  eV,  $N_c \approx 5.7 \times 10^{17} \text{ cm}^{-3}$ ,  $N_v \approx 1.1 \times 10^{19} \text{ cm}^{-3}$ ,  
 $n_i = \sqrt{(5.7 \times 10^{17})(1.1 \times 10^{19})} \exp\left(-\frac{1.344}{2 \times 0.02585}\right) = 1.28 \times 10^7 \text{ cm}^{-3}$ .
2. InGaAs lattice matched to InP ( $\text{Ga}_{0.47}\text{In}_{0.53}\text{As}$ ):  $E_g \approx 0.74$  eV,  
 $N_c \approx 2.1 \times 10^{17} \text{ cm}^{-3}$ ,  $N_v \approx 7.7 \times 10^{18} \text{ cm}^{-3}$ ,  
 $n_i = \sqrt{(2.1 \times 10^{17})(7.7 \times 10^{18})} \exp\left(-\frac{0.74}{2 \times 0.02585}\right) = 7.73 \times 10^{11} \text{ cm}^{-3}$ .

In an intrinsic semiconductor we have  $n_e = n_h$  (charge neutrality). Hence Eqs. 3.14 and 3.17 are identical in this case.

It is noted that in many practical cases the effective electron mass in the conduction band is of the same order as the electron mass  $m_c \approx m$ , whereas the valence band effective mass can be larger than the electron mass,  $m_v > m$ , by a factor 10 or more; “holes are heavier than electrons”. Also note that we have been dealing so far with intrinsic, or pure, semiconductors, for which  $E_F$  is in the center of the energy gap.

### 3.4 Doped semiconductors

A semiconductor consisting of a pure crystal without impurities is called an *intrinsic semiconductor*. The intrinsic semiconductor may be an interesting material, but the real power of semiconductors is realized by adding small controlled amounts of specific dopant, or impurity, atoms. The technique of adding impurity atoms to a semiconductor material to change its conductivity is called *doping*. Doping can significantly alter the electrical characteristics of the semiconductor. The doped material, called an *extrinsic semiconductor*, is essential for fabrication of the various semiconductor devices that we will treat in later chapters. Consider an intrinsic perfect semiconductor crystal from group IV, such as silicon, for which the valence band is filled with electrons. Adding a small fraction of group V atoms to the crystal will add excess electrons without changing the band structure. For these extra electrons, there is room only in the conduction band. Indeed, the energy needed to separate these electrons from their atom is much smaller than the thermal energy  $k_B T$  at room temperature. Hence, these so-called *donor impurity* atoms add electrons to the conduction band without creating holes in the valence band. The resulting semiconductor is referred to as *n-type* (n for negatively charged electron). On the other hand, adding a small fraction of group III atoms will contribute one valency electron less and, by a similar mechanism as for the donor electrons, the missing electron gives rise to a hole in the

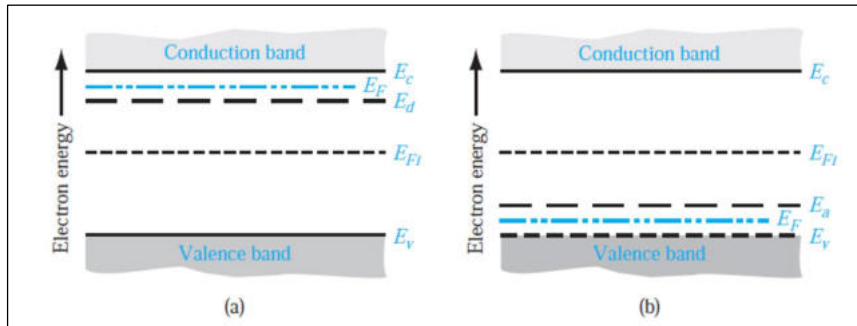


**Figure 3.13:** Simplified energy-band diagrams for (a) n-type and (b) p-type semiconductor at  $T=0$ .  $E_{Fi}$  is the intrinsic Fermi level,  $E_d$  the donor level and  $E_a$  the acceptor level.  $E_c - E_d$  is the binding energy of the outermost electron of the type-V atom;  $E_a - E_v$  is the binding energy of the hole generated by the missing electron of the type-III atom.

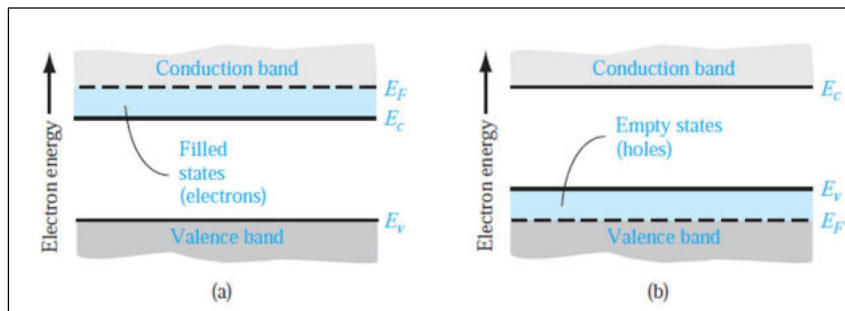


**Figure 3.14:** Simplified energy-band diagrams for (a) n-type and (b) p-type semiconductor at  $T > 0$ .

valence band. These group III atoms are called acceptor impurity atoms. They generate holes in the valence band without adding electrons to the conduction band. The resulting semiconductor is referred to as p-type (p for positively charged hole). The Fermi energy will change if dopant atoms are added. *acceptor impurity*  
*p-type*

For III-V semiconductors group VI atoms may be added as donor atoms, making the material n-type, and group II atoms to make it p-type. Adding group IV atoms can make the material n-type or p-type, dependent on whether they replace a group III or a group V atom in the crystal.

Fig. 3.13 shows schematic simplified energy-band diagrams for n-type and p-type semiconductors at  $T = 0$ . In (a) the excess electrons of the donor atoms occupy the donor energy levels in the bandgap just below the conduction band. The Fermi level is precisely halfway the topmost occupied energy level (the donor level  $E_d$ ) and the conduction band minimum  $E_c$ . In (b) the acceptor atoms give rise to empty acceptor energy levels in the gap just above the valence band. The Fermi energy is now halfway the acceptor level  $E_a$  and the top of the valence band  $E_v$ . The position of the intrinsic Fermi level  $E_{Fi}$  at  $T = 0$  is indicated.

In Fig. 3.14 the situation is sketched in case (a) the donor electrons have been thermally excited to the conduction band and (b) electrons from the valence band have been thermally activated to occupy all acceptor states, leaving behind holes in the uppermost part of the valence band. Since the activation energies are typically small frac-

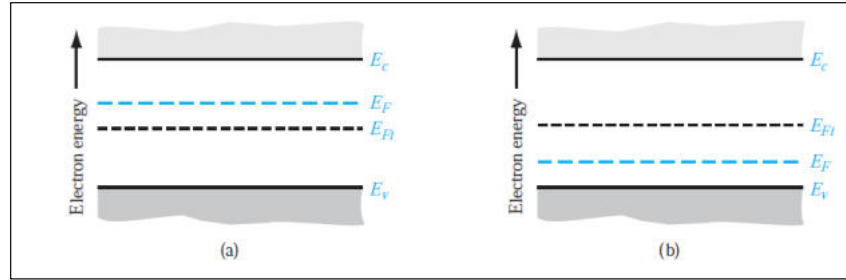


**Figure 3.15:** Position of the Fermi level for (a) n-type ( $N_d > N_a$ ) and (b) p-type ( $N_d < N_a$ ) compensated semiconductor.

tions of the bandgap energy, the thermal activation will be achieved for temperatures much smaller than room temperature.

If a semiconductor contains both donor and acceptor impurities in the same region, it is referred to as compensated semiconductor. In an n-type compensated semiconductor we have  $N_d > N_a$  and in a p-type  $N_d < N_a$ . A completely compensated semiconductor, i.e. with  $N_d = N_a$ , has the characteristics of an intrinsic material. The Fermi level in an n-type compensated semiconductor is in the bandgap and above the intrinsic Fermi level; likewise, in a p-type compensated semiconductor the Fermi level is in the bandgap and below the intrinsic Fermi level. This is schematically indicated in Fig. 3.15.

When we assume that the Fermi energy of the doped semiconductor is within the forbidden-energy bandgap and not too close to  $E_c$  or  $E_v$ , the theory of the previous section applies, and the density  $n_e$  of electrons in the conduction band is given by (see Eq. 3.14)

$$n_e = N_c e^{-\frac{E_c - E_F}{k_B T}},$$

where we have assumed that  $(E_c - E_F) \gg k_B T$ , so that the Fermi probability function reduces to the Boltzmann approximation and  $N_c$  is the effective density of quantum states in the conduction band given by Eq. 3.15. Similarly, in the same approximation the density of holes in the valence band is given by Eq. 3.17,

$$n_h = N_v e^{-\frac{E_F - E_v}{k_B T}},$$

with  $N_v$  the effective density of states in the valence band given by Eq. 3.18.

When the concentration of electrons in the conduction band exceeds the density of states  $N_c$ , the Fermi energy lies within the conduction band. This type of semiconductor is called a degenerate n-type semiconductor. In a similar way, the Fermi energy will lie in the valence band when the concentration of holes exceeds the density of states  $N_v$ . This type of semiconductor is called a degenerate p-type semiconductor. Degenerately doped p and n-type semiconductors are very important in high-speed transistors and in certain types of sensors and detectors. The increased carrier concentration allows for better control of electrical conductivity and enhanced electrical and optical performance of devices.

**Problem 3.3:** Carrier and hole concentrations for the standard waveguide layers.

**Problem:** Calculate the carrier and hole concentrations at room temperature for the following layers of the standard waveguide structure (see Appendix C, Fig. C.2):

1. n-type InP substrate with a doping level of  $10^{18} \text{ cm}^{-3}$
2. n-type Q1.25 waveguide layer with a doping level of  $10^{16} \text{ cm}^{-3}$  ( $d = 500 \text{ nm}$ )
3. p-type InP cladding layer with a doping level of  $10^{18} \text{ cm}^{-3}$  ( $d = 1000 \text{ nm}$ )
4. p-type InGaAs contact layer with a doping level of  $10^{19} \text{ cm}^{-3}$  ( $d = 300 \text{ nm}$ )

**Solution:**

1. The doping level of  $10^{18} \text{ cm}^{-3}$  exceeds the effective density of states at the conduction band ( $N_c \approx 5.7 \times 10^{17} \text{ cm}^{-3}$ ), and therefore, the Boltzmann approximation does not hold anymore. The majority carrier density is approximately the donor concentration:  $n_e \approx N_d = 10^{18} \text{ cm}^{-3}$ . Accurate calculation of the minority carrier concentration requires numerically solving the Fermi-Dirac integral (Eq. 3.13).
2. Q1.25 has a bandgap corresponding to a photon of  $1.25 \mu\text{m}$  wavelength:  $E_g = h\nu = h\frac{c}{\lambda} \approx 0.99 \text{ eV}$ . Q1.25 is  $\text{Ga}_x\text{In}_{1-x}\text{As}_y\text{P}_{1-y}$  lattice matched to InP, or  $[(\text{InP})_{(1-y)}(\text{Ga}_{0.47}\text{In}_{0.53}\text{As})_y]$ . The bandgap can also be expressed with [103]:  $E_g = 1.353(1-y) + 0.737y + 0.13y^2$ . Therefore, the composition can be obtained as:  $y \approx 0.689$ ,  $x = 0.47y \approx 0.324$ . Effective density of states [102]:  $N_c = 2.5 \times 10^{19}(0.08 - 0.039y)^{\frac{3}{2}} \approx 3.1 \times 10^{17} \text{ cm}^{-3}$ ,  $N_v = 2.5 \times 10^{19}(0.6 - 0.18y)^{\frac{3}{2}} \approx 8.2 \times 10^{18} \text{ cm}^{-3}$ . The doping concentration  $N_d = 10^{16} \text{ cm}^{-3}$  is much smaller than the effective density of states, and therefore the semiconductor is non-degenerate, and the Boltzmann approximation can be used. Mass action law (see Problem 3.2):  $n_e n_h = n_i^2 = N_c N_v \exp\left(-\frac{E_g}{k_B T}\right) \approx 5.86 \times 10^{19} \text{ cm}^{-6}$ . Charge neutrality requires:  $n_e + N_d = n_h$ . Therefore,  $n_e = \frac{N_d}{2} + \sqrt{\left(\frac{N_d}{2}\right)^2 + n_i^2} \approx 1.0 \times 10^{16} \text{ cm}^{-3}$  and  $n_h = n_i^2 / n_e \approx 5.86 \times 10^3 \text{ cm}^{-3}$ .
3. Effective density of states [102]:  $N_c \approx 5.7 \times 10^{17} \text{ cm}^{-3}$ ,  $N_v \approx 1.1 \times 10^{19} \text{ cm}^{-3}$ . Since the doping level is much smaller than the valence band effective density of states, the semiconductor is non-degenerate.  $n_e n_h = n_i^2 = N_c N_v \exp\left(-\frac{E_g}{k_B T}\right) \approx 1.65 \times 10^{14} \text{ cm}^{-6}$ . Charge neutrality requires:  $n_e = n_h + N_a$ . Therefore,  $n_h = \frac{N_a}{2} + \sqrt{\left(\frac{N_a}{2}\right)^2 + n_i^2} \approx 1.0 \times 10^{18} \text{ cm}^{-3}$  and  $n_e = n_i^2 / n_h \approx 1.65 \times 10^{-4} \text{ cm}^{-3}$ .
4. The doping level of  $10^{19} \text{ cm}^{-3}$  exceeds the effective density of states at the valence band ( $N_v \approx 7.7 \times 10^{18} \text{ cm}^{-3}$ ), and therefore, the Boltzmann approximation does not hold anymore. The majority carrier density is approximately the acceptor concentration:  $n_h \approx N_a = 10^{19} \text{ cm}^{-3}$ . Accurate calculation of the minority carrier concentration requires numerically solving the Fermi-Dirac integral (Eq. 3.13).

**Problem 3.4:** Square resistance of the standard waveguide layers

**Problem:** Calculate the square resistance of the layers 2-4 from Problem 3.3.

**Solution:** The sheet (square) resistance is  $R_{\square} = \frac{\rho}{t} = \frac{1}{\sigma t}$ , where  $\rho$ ,  $\sigma$ , and  $t$  are the resistivity, conductivity, and thickness of the slab, respectively. For a doped semiconductor in which one carrier dominates,  $\sigma \approx e\mu N$ , where  $e$  is the electron charge,  $\mu$  is the carrier mobility, and  $N$  is the majority-carrier concentration. Hence we have  $R_{\square} = \frac{1}{e\mu N t}$  [ $\Omega/\square$ ]. The mobilities can be calculated using an empirical model [104]:  $\mu_e^{Q1.25} \approx 4872 \text{ cm}^2 \text{ V}^{-1} \text{ s}^{-1}$ ,  $\mu_h^{\text{InP}} \approx 72 \text{ cm}^2 \text{ V}^{-1} \text{ s}^{-1}$ ,  $\mu_h^{\text{InGaAs}} \approx 81 \text{ cm}^2 \text{ V}^{-1} \text{ s}^{-1}$ . Finally, we obtain the square resistances:  $R_{\square}^{Q125} = \frac{1}{(1.602 \times 10^{-19})(4872)(1 \times 10^{16})(5 \times 10^{-5})} \approx 2562 \text{ } \Omega/\square$ ,  $R_{\square}^{\text{InP}} = \frac{1}{(1.602 \times 10^{-19})(72)(1 \times 10^{18})(1 \times 10^{-4})} \approx 867 \text{ } \Omega/\square$ , and  $R_{\square}^{\text{InGaAs}} = \frac{1}{(1.602 \times 10^{-19})(81)(1 \times 10^{19})(3 \times 10^{-5})} \approx 257 \text{ } \Omega/\square$ .

## 3.5 The pn-junction

### 3.5.1 Zero applied bias

We now will study situations where a p-type and an n-type semiconductor are brought into tight contact with each other such that carriers can freely move through the interface, or junction, between the two materials. This configuration is referred to as *pn-junction*. Most semiconductor devices have at least one such (or similar) junction; the device characteristics are intimately connected to these pn-junctions.

Now consider the situation sketched in Fig. 3.16(a), where the left part of a single semiconductor crystal has been doped with acceptor atoms of concentration  $N_a$  and the right part with donor atoms of concentration  $N_d$ . This is referred to as *homojunction*, because the semiconductor crystal is the same left and right of the junction. In this situation we initially have an abrupt change in density of electrons at the interface (Fig. 3.16(b), dashed horizontal lines). In general, carriers will then redistribute by diffusion in such a manner as to reduce the density gradient. Thus, electrons move from the n-region into the p-region, or equivalently, holes move from the p-region into the n-region. Since the structure was initially charge neutral, the consequence of the diffusive charge redistribution is the formation of a dipole layer on both sides of the interface, with negative space charge to the left and positive space charge to the right. This continues until equilibrium is reached where the diffusion force acting on the electrons will be compensated by the counteracting electrostatic Coulomb force induced by the dipole-induced electric field. This is schematically illustrated in Fig. 3.16(c).

The indicated space-charge region is also called *depletion region*. If we assume that no voltage is applied to the pn-junction, then the system will be in thermal equilibrium, which means that the Fermi energy level is constant everywhere in the system. In terms of the band diagram for this situation this means in case of compensated semiconductors, that the conduction and valence bands must bend as we go through the space charge region, as sketched in Fig. 3.17. Far away from the junction the band diagrams are as shown in Fig. 3.15. Here, we will use the index  $i$  to indicate quantities that pertain to the intrinsic, i.e., non-doped semiconductor. The electron concentration in the conduction band of the n-region is (see Eq. 3.14)

$$n_e = N_d = N_c e^{-\frac{E_c - E_F}{k_B T}} = n_i e^{\frac{E_F - E_{Fni}}{k_B T}} = n_i e^{-\frac{e\phi_{Fni}}{k_B T}}, \quad (3.19)$$

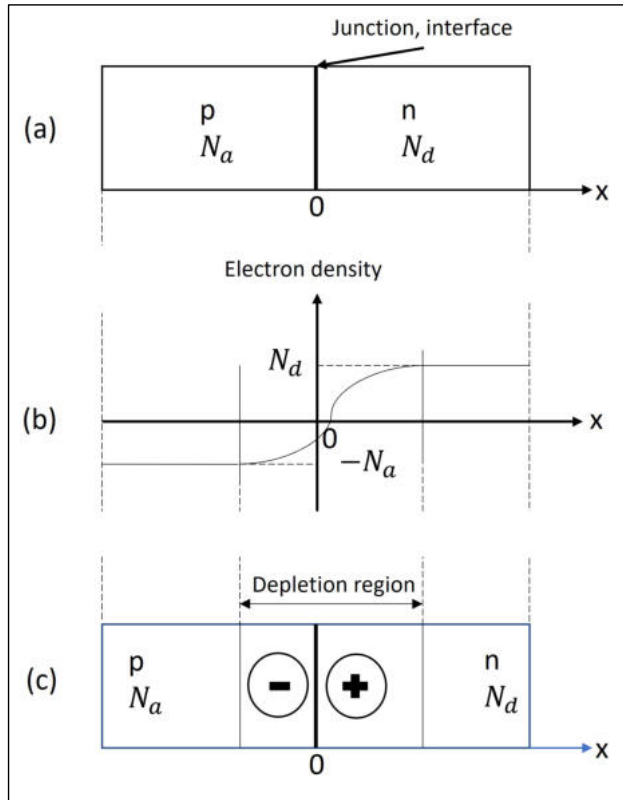


**Figure 3.16:** Charge redistribution when (a) two doped semiconductor crystals are put together to form a pn-junction. In (b) the large density gradient induces diffusion forces driving electrons to the left (and holes to the right), leading to (c) an equilibrium situation with a space-charge or depletion region as indicated.

where  $N_d$  is the donor concentration,  $n_i \equiv N_c e^{-\frac{E_c - E_{Fni}}{k_B T}}$  is the intrinsic carrier concentration with  $E_{Fni}$  the intrinsic Fermi energy in the n-region, and  $\phi_{Fn}$  is defined as (see Fig. 3.17)

$$e\phi_{Fn} \equiv E_{Fni} - E_F. \quad (3.20)$$

Similarly, in the p-region, the hole concentration is

$$n_h = N_a = n_i e^{\frac{E_{Fpi} - E_F}{k_B T}} = n_i e^{\frac{e\phi_{Fp}}{k_B T}}, \quad (3.21)$$

with  $N_a$  the acceptor concentration in the p-region and the potential  $\phi_{Fp}$  is defined (see Fig. 3.17) by

$$e\phi_{Fp} = E_{Fpi} - E_F. \quad (3.22)$$

Electrons in the conduction band of the n-region are blocked by the built-in potential barrier  $V_b$ , as indicated in Fig. 3.17 and similarly for holes in the p region. This barrier is a consequence of thermal equilibrium and maintains equilibrium between majority electrons in the n-region and minority electrons in the p-region, and similarly between majority holes in the p-region and minority holes in the n-region.  $V_b$  can be expressed as the difference between the intrinsic Fermi levels in the p and n-regions in terms of the potentials  $\phi_{Fn}$  and  $\phi_{Fp}$ , i.e.,

$$V_b = |\phi_{Fn}| + |\phi_{Fp}|. \quad (3.23)$$

*built-in potential barrier  $V_b$*

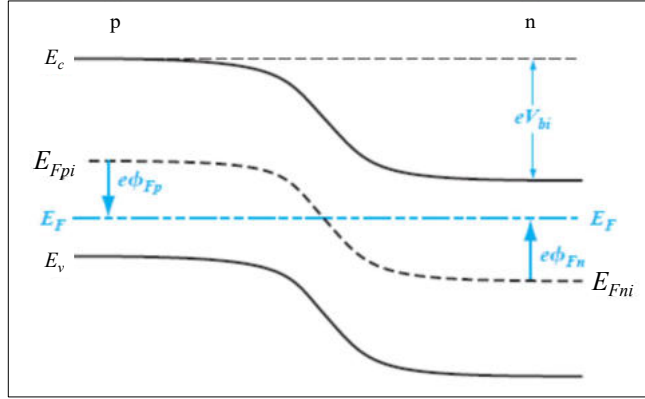


**Figure 3.17:** Energy-band diagram of a pn-junction of compensated semiconductors in thermal equilibrium; no electrical current flows through the structure. Far away from the junction the band diagrams are as shown in Fig. 3.15.

**Problem 3.5:** Calculation of the potential barrier.

**Problem:** Calculate the potential barrier in the InP cladding layer on top of the standard waveguide (see Appendix C, Fig. C.2), with a p-type doping level of  $10^{17}$  and an n-type doping level of  $10^{16}$

**Solution:** According to Eq. 3.26,  $V_b = \frac{k_B T}{e} \ln\left(\frac{N_a N_d}{n_i^2}\right) = \frac{0.02585}{1} \ln\left(\frac{5 \times 10^{17} \times 3 \times 10^{16}}{1.65 \times 10^{14}}\right) \approx 1.19$  V.

According to Eq. 3.19 we can express the potential  $\phi_{Fn}$  as

$$\phi_{Fn} = -\frac{k_B T}{e} \ln\left(\frac{N_d}{n_i}\right) \quad (3.24)$$

with  $N_d$  the donor concentration. Similarly, we can derive from Eq. 3.21

$$\phi_{Fp} = +\frac{k_B T}{e} \ln\left(\frac{N_a}{n_i}\right). \quad (3.25)$$

The built-in potential barrier  $V_b$  for the junction, introduced in Eq. 3.23, can be expressed, using Eqs. 3.23, 3.24 and 3.25 as

$$V_b = \frac{k_B T}{e} \ln\left(\frac{N_a N_d}{n_i^2}\right) = V_T \ln\left(\frac{N_a N_d}{n_i^2}\right) \quad (3.26)$$

*thermal voltage* where  $V_T \equiv \frac{k_B T}{e}$  is the thermal voltage.

### 3.5.2 Space charge width in the junction area

In Fig. 3.16, the depletion region around the pn-junction was introduced. This region is characterized by space charge, which is illustrated in Fig. 3.18, where we have assumed that the space-charge region abruptly ends in the n-region at  $x = x_n$  and in the p-region

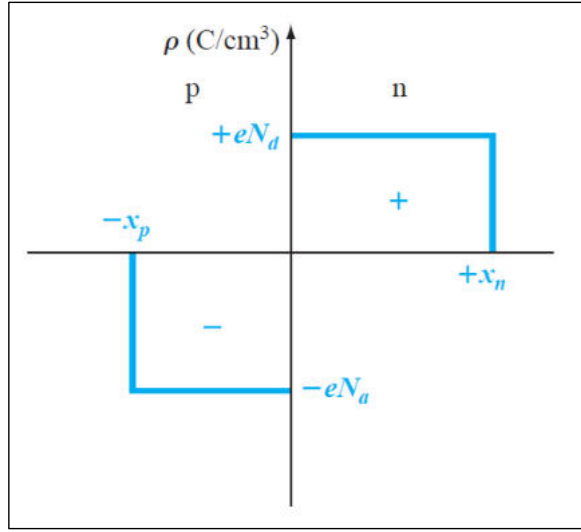


**Figure 3.18:** Space charge density corresponding to the abrupt junction approximation in Fig. 3.16(c).

at  $x = -x_p$  ( $x_p > 0$ ). We denote the electric potential by  $\phi(x)$  which is related to the charge density  $\rho(x)$  by the Poisson equation (in 1 dimension)

$$\frac{d^2\phi(x)}{dx^2} = -\frac{\rho(x)}{\epsilon_s}, \quad (3.27)$$

with  $\epsilon_s$  the permittivity of the semiconductor where  $\epsilon_s = \epsilon_r \epsilon_0$  is the permittivity of the semiconductor,  $\epsilon_r$  the relative permittivity of the semiconductor and  $\epsilon_0$  the permittivity of vacuum. The charge density is (see Fig. 3.18)

$$\rho(x) = \left\{ \begin{array}{ll} 0 & , \quad x < -x_p \text{ \& } x > x_n \\ -eN_a & , \quad -x_p < x < 0 \\ eN_a & , \quad 0 < x < x_n \end{array} \right\}. \quad (3.28)$$

Note that, because of charge neutrality, we must have

$$N_a x_p = N_d x_n, \quad (3.29)$$

and the boundary conditions (see Fig. 3.17) are (37)

$$\phi(x) = \left\{ \begin{array}{ll} 0 & , \quad x < -x_p \\ V_b & , \quad x > x_n \end{array} \right\}. \quad (3.30)$$

It can easily be verified that the solution of Eq. 3.27 with Eq. 3.28, which is continuous, and satisfies Eq. 3.30, is given by

$$\phi(x) = \left\{ \begin{array}{ll} \frac{eN_d}{2\epsilon_s} (x + x_p)^2 & , \quad -x_p < x < 0 \\ \frac{eN_d}{\epsilon_s} (x_n x - \frac{1}{2} x^2) + \frac{eN_d}{2\epsilon_s} x_p^2 & , \quad 0 < x < x_n \end{array} \right\}. \quad (3.31)$$

Therefore, since  $V_b = \phi(x_n) - \phi(-x_p) = \phi(x_n)$ , we have (39)

$$V_b = \frac{e}{2\epsilon_s} (N_d x_n^2 + N_a x_p^2). \quad (3.32)$$

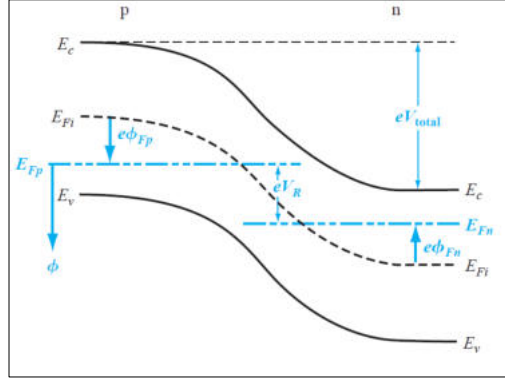


**Figure 3.19:** Energy-band diagram of a pn-junction under reverse bias  $V_R$

The built-in potential is through Formula 3.31 related to the space-charge penetration distances  $x_n$  and  $x_p$ . Combined with Eq. 3.29 we can solve for  $x_n$  and  $x_p$ ,

$$x_n = \sqrt{\frac{2\epsilon_s V_b}{e} \frac{N_a}{N_d(N_a + N_d)}}, \quad (3.33)$$

$$x_p = \sqrt{\frac{2\epsilon_s V_b}{e} \frac{N_d}{N_a(N_a + N_d)}} \quad (3.34)$$

The total width  $W$  of the space-charge region can then be expressed as

$$W = x_n + x_p = \sqrt{\frac{2\epsilon_s V_b}{e} \frac{(N_a + N_d)}{N_a N_d}} \quad (3.35)$$

Note that  $V_b$  is given by Eq. 3.26.

### 3.5.3 Reverse applied bias, junction capacitance and reverse current

If a positive potential is applied between the p and n regions, the system will no longer be in thermal equilibrium. Far away from the junction each part, n or p, will be in local equilibrium with its own Fermi level. The two Fermi levels,  $E_{Fp}$  and  $E_{Fn}$  will now differ by the applied voltage  $eV_R$ , as indicated in the sketched energy band diagram under reverse bias in Fig. 3.19.

Hence, the total internal barrier height  $V_{total}$  is now given by

$$V_{total} = V_b + V_R. \quad (3.36)$$

A consequence of the applied voltage  $V_R$  is that additional charge has displaced to enlarge the space charge region, the width of which is again given by Eq. 3.35 with  $V_b$  replaced by  $V_{total}$ , i.e.,

$$W = \sqrt{\frac{2\epsilon_s (V_b + V_R)}{e} \frac{(N_a + N_d)}{N_a N_d}}. \quad (3.37)$$

The width of the space-charge region has increased due to the reverse bias. This increase of the total electric charges around the interface of the pn-junction means that a capacitance  $C_{pn}$  can be assigned to the junction. It is defined as

$$C_{pn} = \frac{dQ}{dV_R}, \quad (3.38)$$

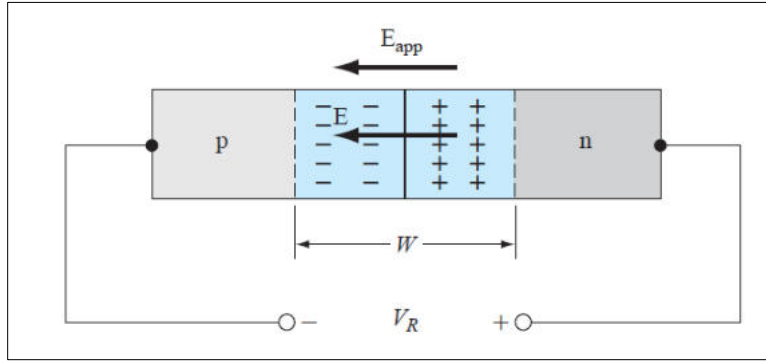


**Figure 3.20:** A pn-junction with applied reverse bias voltage  $V_R > 0$ , showing the direction of the current and the induced electric field.

where  $Q$  is the displaced charge, see Eq. 3.29

$$Q = eN_a x_p = eN_d x_n \quad (3.39)$$

For the barrier under reverse bias we can write, using Eq. 3.33,

$$x_n = \sqrt{\frac{2\epsilon_s(V_b + V_R)}{e} \frac{N_a}{N_d(N_a + N_d)}}. \quad (3.40)$$

The junction capacitance can now be written, using Eqs. 3.38-3.40 as

$$C_{pn} = eN_d \frac{dx_n}{dV_R} = \sqrt{\frac{e\epsilon_s}{2(V_b + V_R)} \frac{N_a N_d}{(N_a + N_d)}}. \quad (3.41)$$

It is also referred to as depletion-layer capacitance.

The effective built-in potential-energy barrier is  $eV_{total} = e(V_b + V_R)$ , with  $V_R$  the applied reverse bias voltage, see Fig. 3.19. Here, the positive pole is connected to the n-side and the negative pole to the p-side, see Fig. 3.20. The only way carriers can pass this barrier is by thermal activation, for which the probability is proportional to the Boltzmann factor  $e^{-\frac{e(V_b + V_R)}{k_B T}}$ . To deduce the dependence on  $V_R$  of the current that flows across the pn-junction, we must consider separately the electrical currents of electrons and holes,  $j_e$  and  $j_h$ , respectively. When  $V_R = 0$ , both  $j_e$  and  $j_h$  vanish, since the system is in thermal equilibrium. This does not, of course, mean that no individual carriers flow across the junction, but rather that as many electrons (or holes) flow in one direction as in the other. This balance is disrupted when  $V_R \neq 0$ . Consider, for example, the electrical current of holes across the depletion layer, which has two components:

1. Holes flow from the n- to the p-side of the junction leading to an electrical current known as the hole generation current. This current arises from holes that are generated just on the n-side of the depletion layer by thermal excitation of electrons out of the valence band. Although the density of such holes on the n-side ("minority carriers") is very small compared with the density of electrons ("majority carriers"), they play an important role in carrying current across the junction. This is because any such hole that wanders into the depletion layer is immediately swept over to the p-side of the junction by the strong electric field that prevails within the layer. The resulting generation current is insensitive to the size of the potential drop across the depletion layer, since any hole, having entered the layer from the n-side, will be swept through to the p-side.

2. Holes flow from the p- to the n-side of the junction leading to an electrical current known as hole recombination current. This name stems from the fact that such holes upon arriving on the n-side of the junction will quickly recombine with one of the abundant electrons. Since these holes have to move against the potential barrier the number of successful holes is proportional to the Boltzmann factor  $e^{-\frac{e(V_b+V_R)}{k_B T}}$  and the corresponding electrical current density satisfies

$$j_h^{rec} \propto e^{-\frac{e(V_b+V_R)}{k_B T}}. \quad (3.42)$$

In contrast to the generation current, the recombination current is highly sensitive to the applied (reverse) voltage  $V_R$ . Since at  $V_R = 0$ , there can be no net hole current across the junction, we have

$$j_h^{rec} = j_h^{gen} e^{-\frac{eV_R}{k_B T}}. \quad (3.43)$$

The total hole electrical current density flowing through the junction in the np-direction is given by the generation current minus the recombination current,

$$j_h = j_h^{gen} - j_h^{rec} = j_h^{gen} (1 - e^{-\frac{eV_R}{k_B T}}). \quad (3.44)$$

The same analysis applies to the components of the electron current, except that the generation and recombination currents for electrons flow oppositely to the corresponding hole currents. However, since electrons are oppositely charged, the electrical currents are parallel, thus leading to the total (reverse) electrical current density in the np-direction given by

$$J_R = (j_h^{gen} + j_e^{gen})(1 - e^{-\frac{eV_R}{k_B T}}) \equiv J_S^0 (1 - e^{-\frac{eV_R}{k_B T}}), \quad (3.45)$$

valid for

$$V_R \geq 0 \quad (3.46)$$

and where  $J_S^0 = j_h^{gen} + j_e^{gen}$  is a material-specific current, the reverse-saturation current density,

$$J_S^0 \propto e^{-\frac{eV_b}{k_B T}} \quad (3.47)$$

Note that for increasing  $V_R$ , the reverse current saturates at the value  $J_S^0$ .

### 3.5.4 Forward applied bias: the pn-junction diode

In case of forward bias voltage  $V_a$ , Equation 3.45 with  $V_R$  replaced by  $-V_a$  yields for the forward current flowing in the pn direction (see the inset of Fig. 3.21)

$$J = J_S^0 (e^{\frac{eV_a}{k_B T}} - 1), \quad (3.48)$$

valid as long as the effective barrier  $V_b - V_a$  exists, i.e.,  $V_a < V_b$ . The current density is plotted in Fig. 3.21 as a function of the applied forward-bias voltage  $V_a$ , which can assume negative values as well. Equation 3.48 is known as the ideal-diode equation. In the derivation of the ideal current-voltage relationship, we neglected any effects occurring within the space-charge region. These effects cause the I-V relationship to deviate substantially from the ideal expression. The effects in question are related to the presence of trap levels within the bandgap, which provide the dominant mechanism for electron and hole generation in the junction region. With these traps as intermediate

**Problem 3.6:** Depletion layer properties.

**Problem a):** Estimate the width of the depletion layer in the standard waveguide layer for a reverse bias voltage  $V_b = 0, 1$  and  $5$  V.

**Solution a):** The standard waveguide has a p-n homojunction between p-InP and n-InP. The material properties are:  $\epsilon_r = 12.5$  [102],  $N_d = 3 \times 10^{16} \text{ cm}^{-3}$ ,  $N_a = 5 \times 10^{17} \text{ cm}^{-3}$ . The depletion layer width can be calculated with Eq. 3.35:

$$W = \sqrt{\frac{2\epsilon_s(V_b+V_R)}{e} \frac{N_a+N_d}{N_a N_d}}. \quad V_b \text{ can be obtained from Problem 3.3: } V_b \approx 1.19 \text{ V. Let}$$

$$N^* = \frac{N_a N_d}{N_a + N_d} = \frac{5 \times 10^{17} \times 3 \times 10^{16}}{5 \times 10^{17} + 3 \times 10^{16}} \approx 2.83 \times 10^{16} \text{ cm}^{-3}, \text{ then}$$

$$W_{0V} = \sqrt{\frac{2 \times 12.5 \times 8.854 \times 10^{-12} (1.19+0)}{1.602 \times 10^{-19} \times 2.83 \times 10^{16} \times 10^6}} \approx 241 \text{ nm},$$

$$W_{1V} = \sqrt{\frac{2 \times 12.5 \times 8.854 \times 10^{-12} (1.19+1)}{1.602 \times 10^{-19} \times 2.83 \times 10^{16} \times 10^6}} \approx 327 \text{ nm},$$

$$W_{5V} = \sqrt{\frac{2 \times 12.5 \times 8.854 \times 10^{-12} (1.19+5)}{1.602 \times 10^{-19} \times 2.83 \times 10^{16} \times 10^6}} \approx 550 \text{ nm}$$

**Problem b):** Estimate the capacitance of the depletion layer in the standard modulator based on the standard waveguide layer. with a width of  $2 \mu\text{m}$  and a length of  $500 \mu\text{m}$ , for a reverse bias voltage  $V_b = 0, 1$  and  $5$  V.

**Solution b):** The junction capacitance can be calculated using Eq. 3.41:

$$C_{pn} = \sqrt{\frac{e\epsilon_s}{2(V_b+V_R)} \frac{N_a N_d}{N_a + N_d}} = \sqrt{\frac{e\epsilon_s}{2(V_b+V_R)}} N^*. \text{ The area is}$$

$$A = W \times L = 2 \times 500 = 1000 \mu\text{m}^2. \text{ Therefore, } C_{0V} = C_{pn} \times A =$$

$$\sqrt{\frac{1.602 \times 10^{-19} \times 12.5 \times 8.854 \times 10^{-12}}{2 \times (1.19+0)}} \times 2.83 \times 10^{16} \times 10^6 \times 1000 \times 10^{-12} \approx 0.46 \text{ pF},$$

$$C_{1V} = C_{pn} \times A = \sqrt{\frac{1.602 \times 10^{-19} \times 12.5 \times 8.854 \times 10^{-12}}{2 \times (1.19+1)}} \times 2.83 \times 10^{16} \times 10^6 \times 1000 \times 10^{-12} \approx$$

$$0.34 \text{ pF}, \quad C_{5V} = C_{pn} \times A =$$

$$\sqrt{\frac{1.602 \times 10^{-19} \times 12.5 \times 8.854 \times 10^{-12}}{2 \times (1.19+5)}} \times 2.83 \times 10^{16} \times 10^6 \times 1000 \times 10^{-12} \approx 0.20 \text{ pF}$$

**Problem 3.7:** Crosstalk between MZI modulators.

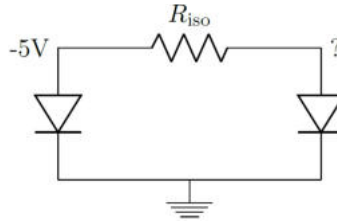
**Problem c):** Estimate the resistance of the path between two standard phase modulators in the arms of a Mach-Zehnder Interferometer, which are connected to an MMI coupler with waveguide sections of  $100 \mu\text{m}$  long, if the  $1 \mu\text{m}$  thick p-doped InP top layer is present (1) or removed (2).

**Solution c):** Since the width of the MMI is much smaller than the waveguide length, the resistance of the MMI can be ignored for this estimation. Consider a symmetric MZI, the path length between two electrodes is  $100 \times 2 = 200 \mu\text{m}$ . Now we calculate the resistivity values for the  $10^{18} \text{ cm}^{-3}$  p-doped InP and the  $5 \times 10^{17} \text{ cm}^{-3}$  p-doped InP. First, the mobilities are calculated using an empirical model [104]:  $\mu_h^{\text{p-InP}10^{18}} \approx 72 \text{ cm}^2 \text{ V}^{-1} \text{ s}^{-1}$  and  $\mu_h^{\text{p-InP}5 \times 10^{17}} \approx 89 \text{ cm}^2 \text{ V}^{-1} \text{ s}^{-1}$ . Since  $\rho = \frac{1}{e\mu N}$ , we have  $\rho_{\text{InP}10^{18}} = 1/(1.602 \times 10^{-19} \times 72 \times 10^{18}) \approx 867 \Omega \mu\text{m}$  and  $\rho_{\text{InP}5 \times 10^{17}} = 1/(1.602 \times 10^{-19} \times 89 \times 5 \times 10^{17}) \approx 1403 \Omega \mu\text{m}$ . With the  $10^{18} \text{ cm}^{-3}$  p-InP:  $R = 1/(\frac{1}{867 \times 200/(1 \times 2)} + \frac{1}{1403 \times 200/(0.3 \times 2)}) \times \frac{1}{2} \approx 36.57 \text{ k}\Omega$ . Without the  $10^{18} \text{ cm}^{-3}$  p-InP:  $R = 1403 \times 200/(0.3 \times 2) \times \frac{1}{2} \approx 233.83 \text{ k}\Omega$ . Here, the  $\frac{1}{2}$  comes from the symmetric input and output waveguides of the MZI.

**Problem d):** Calculate the leakage current if one electrode is grounded and the other is biased at  $-1 \text{ V}$ , if the  $1 \mu\text{m}$  thick p-doped InP top layer is present (1) or removed (2).

**Solution d):** With the  $10^{18} \text{ cm}^{-3}$  p-InP:  $I = \frac{V}{R} = \frac{1}{36.57 \times 10^3} \approx 27.34 \mu\text{A}$ . Without the  $10^{18} \text{ cm}^{-3}$  p-InP:  $I = \frac{V}{R} = \frac{1}{233.83 \times 10^3} \approx 4.28 \mu\text{A}$ .

**Problem e):** Estimate the voltage at the second modulator, if the first one is biased at  $-5 \text{ V}$  and the second one is floating, as depicted in the equivalent circuit below.



**Solution e):** The voltage at the floating modulator can be calculated using the Kirchoff's law:  $\frac{V_a - V_b}{R_{\text{iso}}} + \frac{V_b - 0}{R_{\text{diode}}} = 0$ , where  $V_a = -5\text{V}$ ,  $V_b$  is the voltage on the second modulator, and  $R_{\text{diode}}$  is the reverse-biased diode resistance.  $V_b$  can be solved as:  $V_b = V_a \frac{R_{\text{diode}}}{R_{\text{diode}} + R_{\text{iso}}}$

**Comment** Yi Wang:  $R_{\text{diode}}$  is hard to estimate without knowing diffusion coefficients and carrier lifetimes. Can we put a typical (measured) reverse resistance here?

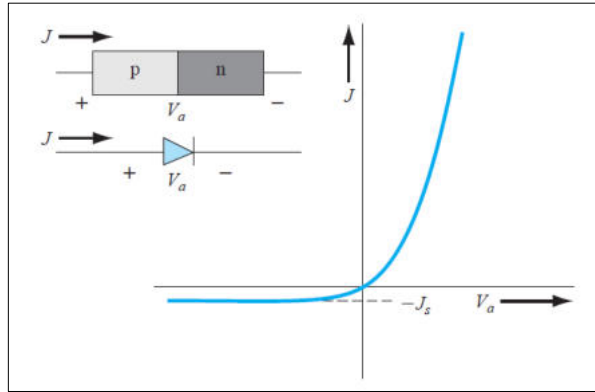


**Figure 3.21:** I-V characteristic of a pn junction diode.

states, the contribution to the recombination (forward) current can then be derived as (Neamen, Ch.8.2[105])

$$j^{rec} = j_{r0} e^{\frac{eV_a}{2k_B T}}, \quad (3.49)$$

where  $j_{r0}$  is the corresponding reverse-biased saturation current density, which is, in contrast to the ideal current case, not independent of the applied voltage, since it depends on the depletion width  $W$ , which in turn depends on the reverse bias voltage (see Eq. 3.35). In reality, the reverse-bias saturation current can be orders of magnitude larger than the ideal current  $J_S$  (see Neamen [105], Ch. 8.2.1). Usually, the total forward-bias current density is cast in a general form, similar to Eq. 3.48,

$$J_{tot} = J_S^{tot} (e^{\frac{eV_a}{nk_B T}} - 1), \quad (3.50)$$

where the parameter  $n$  is called the ideality factor. For large forward-bias voltage,  $n = 1$  and for low forward-bias voltage,  $n = 2$ .

## 3.6 Electro-optic effects

The presence of this electric field will induce an effect on the optical properties of this waveguide. Depending on the bandgap energy and type of the core material (bulk or multiple quantum wells) the waveguide modulator can operate in electro-refractive or electro-absorptive modes.

We first discuss effects for electro-refraction. In particular, linear (Pockels) and quadratic (Kerr) electro-optic effects will occur and change the refractive index of the material locally. Together with carrier-induced (plasma dispersion and band filling) electro-optic effects, the modulation of the depletion thickness and electric field strength leads to a modulation of the local refractive index [106, 107]. This is used to change the phase experienced by the optical signal passing through the phase-shifter section. Each of the mentioned effects can be estimated for the COBRA layer composition and their influence on the refractive index is summed up as

$$\Delta n = \Delta n_{\text{Pockels}} + \Delta n_{\text{Kerr}} + \Delta n_{\text{plasma}} + \Delta n_{\text{BF}}. \quad (3.51)$$

From Fig. 17.2c, it can be seen that not all regions of the optical mode experience the refractive index change equally. To account for this effect, the overlap between the intensity distribution  $I(z)$  and the refractive index change  $\Delta n(z)$  has to be taken into account and an effective index change can be calculated as [106]:

$$\Delta n_{\text{eff}} = \frac{\int_{-\infty}^{\infty} \Delta n(z) \cdot I(z) dz}{\int_{-\infty}^{\infty} I(z) dz}. \quad (3.52)$$

With the electric field dependence on the spatial variable  $z$  and knowledge of the depletion thickness for any given voltage, the above integral can be evaluated for the reverse biased p-i-n junction for each individual electro-optic effect.

### 3.6.1 Electro-refraction in bulk

The properties of a material, in particular the refractive index  $n(E)$  is a function of an externally applied field  $E$ . Several physical effects contribute to the total change of refractive index in the InP/InGaAsP material system [106]:

**Linear electro-optic effect (Pockels Effect)** The linear electro-optic effect acts anisotropically and gives only a refractive index change to TE polarized light and does not affect the TM polarization. Furthermore its sign depends on the light propagation direction and is positive for  $\langle 1\bar{1}0 \rangle$  and negative for the  $\langle 110 \rangle$  direction. It depends linearly on the external field  $E$ :

$$\Delta n_{\text{Pockels}} = \frac{1}{2} n^3 r_{41} E, \quad (3.53)$$

with  $n$  the background index of refraction and  $r_{41}$  the Pockels coefficient. The external field induces stress and strain in the crystal, leading to a change in its index of refraction. Theoretical estimation of the Pockels coefficient is possible using the model of Adachi for a specific  $y$ -composition of the quaternary and InP material and specified wavelengths [108]. Here, we use values from experimental work where the coefficients have been found to be  $r_{41} = 1.4 \cdot 10^{-12}$  m/V in bulk InP [109] and  $r_{41} = 1.6 \cdot 10^{-12}$  m/V in Q-1.25 [110]. This also agrees well with the values reported previously obtained from experiments on COBRA platform phase-shifters [111].

**Quadratic electro-optic effect (Kerr Effect)** The Kerr effect describes a change in the index of refraction which quadratically depends on the applied field. In case the electric field is parallel to the optical field (TM polarization) the index change is given by:

$$\Delta n_{\text{Kerr}} = \frac{1}{2} n^3 r_{11} E^2, \quad (3.54)$$

and in case it is perpendicular to the optical field (TE polarization):

$$\Delta n_{\text{Kerr}} = \frac{1}{2} n^3 r_{12} E^2. \quad (3.55)$$

This change in InP and InGaAsP material comes primarily from the Franz-Keldysh effect which changes the bandgap shape and thus the optical absorption under the presence of an external electric field [112, 113]. Light can be absorbed at energy levels below the bandgap when an excited electron tunnels into the conduction band which is bend under the external electric field. The Kramers-Kronig relation dictates a change of refractive index then due to the absorption

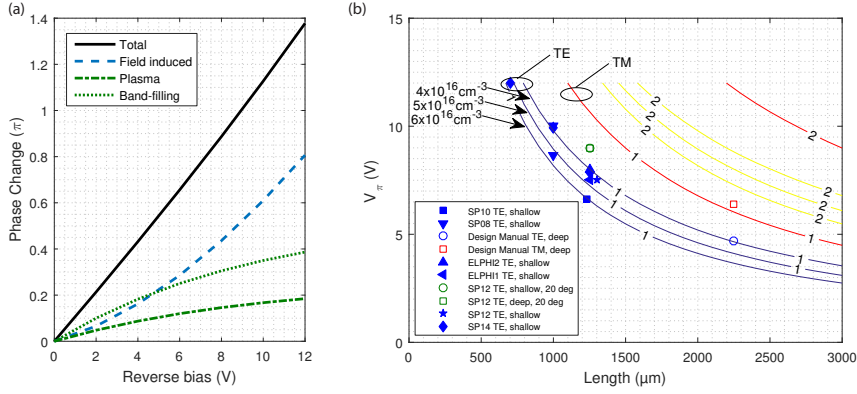


Figure 3.22: &lt;missing caption&gt;

change. This effect does not depend on the propagation direction of light. The values for the Kerr coefficients are  $11.9 \cdot 10^{-20} \text{ m}^2/\text{V}^2$  for TE polarization in Q-1.25 material at  $1.55 \mu\text{m}$  and  $21.5 \cdot 10^{-20} \text{ m}^2/\text{V}^2$  for TM polarization and have been taken from [111] where experimental data on COBRA phase-shifters was used to obtain the values.

**Plasma effect** The plasma effect is related to carrier transitions to higher energy levels inside the same band. During such a process, the carrier density changes and causes a variation of the refractive index. There is a linear dependence of this index change with the doping concentration  $N_d$  according to [106, 107]:

$$\Delta n_{\text{plasma}} = A(E)N_d = \frac{N_d \lambda^2 e^2}{8\pi^2 \epsilon_0 c^2 n \cdot m}, \quad (3.56)$$

with  $e$  the electron charge,  $c$  vacuum velocity of light,  $n$  the initial refractive index and  $m$  the effective mass for electrons or holes. The wavelength dependence is given with  $\lambda$  and the electric field dependence is implied in the carrier concentration. By reverse biasing the pn junction, carriers are depleted and a reverse plasma effect leads to a refractive index change. Its strength has been identified for the COBRA platform to be  $A(E) = 3.65 \cdot 10^{-27} \text{ m}^3$  for InP and  $A(E) = 5.7 \cdot 10^{-27} \text{ m}^3$  in Q-1.25 [111, 114].

**Band-filling effect** This effect is due to the filling of empty energy states in the bands by free carriers, which causes a decrease in optical absorption. This leads again to a change in refractive index. As this effect depends on the carrier concentration, reverse biasing the pn-junction causes a reverse band-filling effect which is proportional to the carrier concentration with the factor:

$$\Delta n_{\text{BF}} = A_{\text{BF}} \cdot N_d \quad (3.57)$$

with  $A_{\text{BF}} = 5 \cdot 10^{-21} \text{ cm}^3$  in InP and  $A_{\text{BF}} = 14 \cdot 10^{-21} \text{ cm}^3$  in Q-1.25 at  $1.55 \mu\text{m}$ . These values have been obtained from [111, 114] and are in good agreement with theoretical predictions using the model by Bennet [107].

Using above descriptions of the effects, the phase change can be evaluated for varying reverse bias voltages. Fig. 3.22a shows the calculation result for a 1 mm long phase-shifter based on the shallow waveguide. The metric  $V_\pi$  is an important measure for electro-refractive modulators and gives the voltage required to reach  $\pi$  phase change.

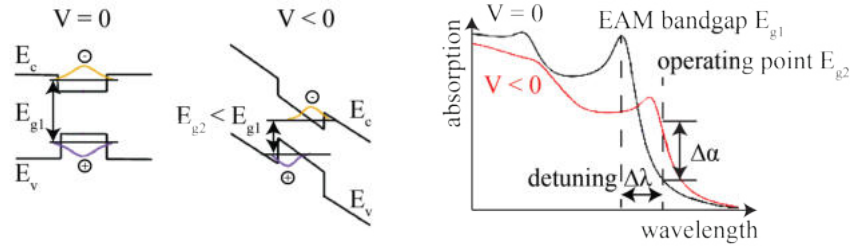


**Figure 3.23:** (left) Electron-hole interaction in a quantum well for no and applied external electric field. (right) Quantum-confined Stark effect: absorption versus wavelength.

Fig. 3.22b displays the calculation result of how  $V_{\pi}$  varies with modulator length and core layer doping concentration. Several experimentally obtained data points are plotted. Such generated graphs for a specific layer stack can aid the design for waveguide modulators.

### 3.6.2 Electro-absorption in bulk

So far, we discussed modeling methodologies for estimating the electro-refraction inside bulk waveguide modulators. This is the case when the core bandgap energy is much higher than that of the operating laser signal. One can use the bulk quaternary core also for electro-absorption when designing for a bandgap energy close to that of the operating laser signal. A similar methodology can be used to estimate the electro-absorption from such structures. However, instead of the Pockels and Kerr effects, one has to estimate the Franz-Keldysh Effect, a field dependent electro-absorption, next to the already discussed bandfilling and plasma effects. We refer to [107] for details on the calculation. Modern electro-absorption modulators (as well as Mach-Zehnder modulators) don't use bulk core but a core consisting of multiple quantum wells sandwiched between quantum barriers because of an enhanced electro-absorption efficiency due to the quantum confinement.

### 3.6.3 Multiple Quantum-Wells (MQW)

The standard COBRA waveguide bulk core can be replaced by a core with multiple quantum well layers during active-passive regrowth. Similar to the quantum well stacks for active devices, tailored quantum wells can be regrown for modulator devices. Multiple regrowth steps can then extend the functionality of the platform and keep the same waveguide core layer dimensions. Detailed discussion of multiple quantum wells can be found in [115]. MQW structures can enhance the electro-absorption and electro-refraction with respect to the bulk waveguide case. In the multi-quantum well structure strong exciton peaks are observed due to two-dimensional confinement, caused by differences in the conduction and valence band energies of the barrier with respect to the well. The exciton represents the Coulomb interaction between the electron-hole pair in a crystal. With an applied electric field the exciton energy shifts, changing the material absorption edge [116]. At the operating point, shown in Fig. 3.23, the absorption increases significantly with the electric field increase. This phenomenon is called the quantum-confined Stark effect (QCSE). The QCSE is observed even at room temperature due to a high binding energy in a confined structure.

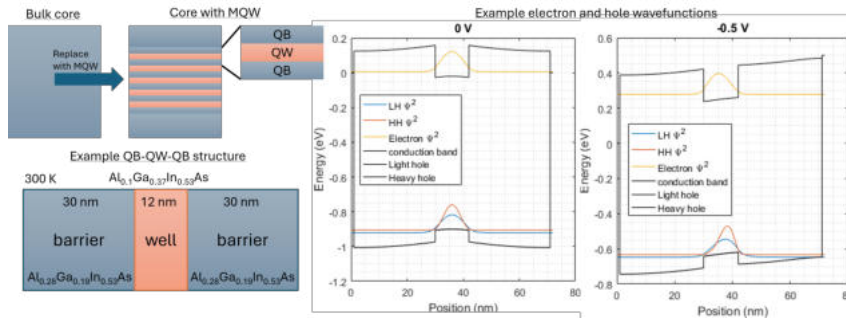


Figure 3.24: <missing caption>

The incident optical signal has a lower bandgap  $E_{g2}$  (higher wavelength) than the modulator structure  $E_{g1}$ , making the modulator transparent when no bias is applied ( $V = 0$ ). The loss which occurs in this case is referred to as the on-state insertion loss  $IL_{ON}$ . When a reverse bias is applied ( $V < 0$ ), the absorption edge shifts to lower energy (higher wavelength) and the incoming light is absorbed. The wavelength difference between the modulator and the laser bandgap is called the detuning wavelength  $\Delta\lambda$ .

Looking at the absorption curve two peaks are observed at different wavelengths. The reason are different exciton energies of heavy-hole (small energy gap) and light-hole (large energy gap) exciton transitions. The heavy/light hole difference makes the modulator polarization dependent, where the heavy-hole corresponds to the TE polarization and light-hole to the TM polarization. The waveguide in generic photonic integration platform is designed to support the TE mode propagation.

This is further illustrated in Fig. 3.24 where a simple two barrier one quantum well system is simulated. The simulation is conducted in the tool Nextnano, a self-consistent quantum mechanics solver which can calculate the conduction and valence band energy levels with the respective electron and hole wavefunctions. The shift of the wavefunction and tilt of energy bands is clearly visible with applied external field.

The QCSE leads to an electric field dependent absorption. The refractive index change and absorption change in the material is linked through the Kramers-Kronig relation [117]. Therefore, the refractive index is also altered through the external field. Depending on the wavelength detuning to the bandedge, the QCSE in MQW is used in electro-absorption ( $\sim 10$  nm detuning) or electro-refractive modulators ( $\sim 100$  nm detuning).

An important parameter for EAM operation is its DC bias voltage  $V_{DC}$ . The lower the value, the lower the total power consumption. For dynamic measurements it is desirable to be positioned in the centre of transmission response linear region (inflection point). In this case the transmission curve is linear and irrelevant of the modulation format at the input  $V(t)$ , its transfer signal will be linear at the output  $T(t)$ . The required swing voltage  $\Delta V$  should also be small to reduce the overall power consumption. In principle, steeper transfer curve needs lower swing. Main parameters influencing the optical signal propagation are: intrinsic layer (i-InP) thickness  $d$ , waveguide width  $w$ , optical confinement factor in MQW  $\Gamma$ , and structure length  $L$ . These parameters will determine the behavior of the EAM and the shape of the transfer curve.

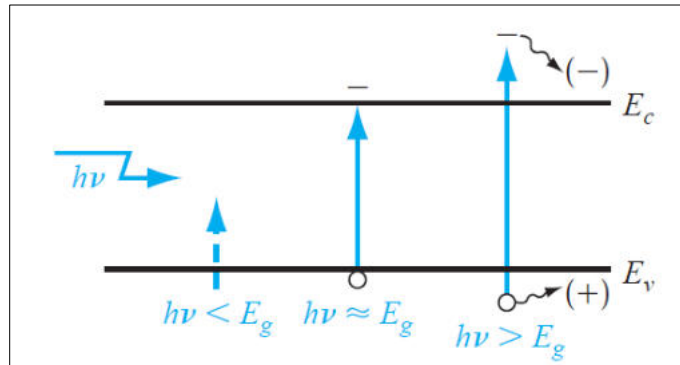


**Figure 3.25:** Optically generated e-h pair formation in a semiconductor when  $h\nu > E_g$ . When  $h\nu < E_g$ , no absorption occurs.

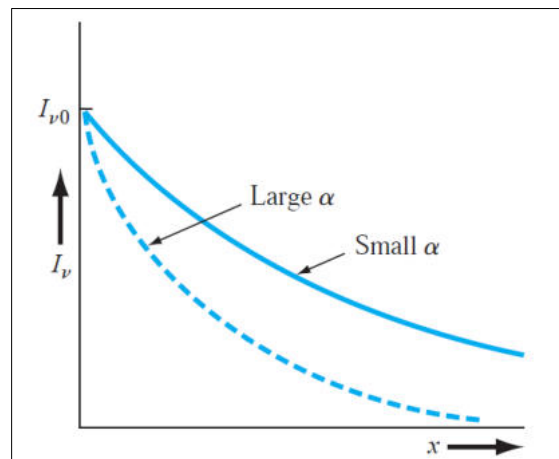


**Figure 3.26:** Photon intensity versus distance for two absorption coefficients.

## 3.7 Light emission and absorption in semiconductor devices

### 3.7.1 Optical absorption

When a semiconductor is illuminated with light, the photons may be absorbed or they may propagate through the semiconductor, depending on the photon energy and on the bandgap energy  $E_g$ . If the photon energy is less than  $E_g$ , the photons are not absorbed, but the light is transmitted through the material; the semiconductor appears to be transparent. Photons with  $E = h\nu > E_g$  can interact with valence electrons and elevate the electrons into the conduction band. The valence band contains many electrons and the conduction band contains many empty states, so this interaction occurs with high probability, each photon creating one electron in the conduction band and one hole in the valence band, i.e., an electron-hole (e-h) pair. The basic absorption processes for different values of  $h\nu$  are shown in Figure 3.25. When  $h\nu > E_g$ , an electron-hole pair is created, and the excess energy may give the electron or hole additional kinetic energy, which will be dissipated as heat in the semiconductor.

As a result of the absorption process, the intensity of the photon flux, denoted by  $I_\nu(x)$

*electron-hole (e-h)  
pair*

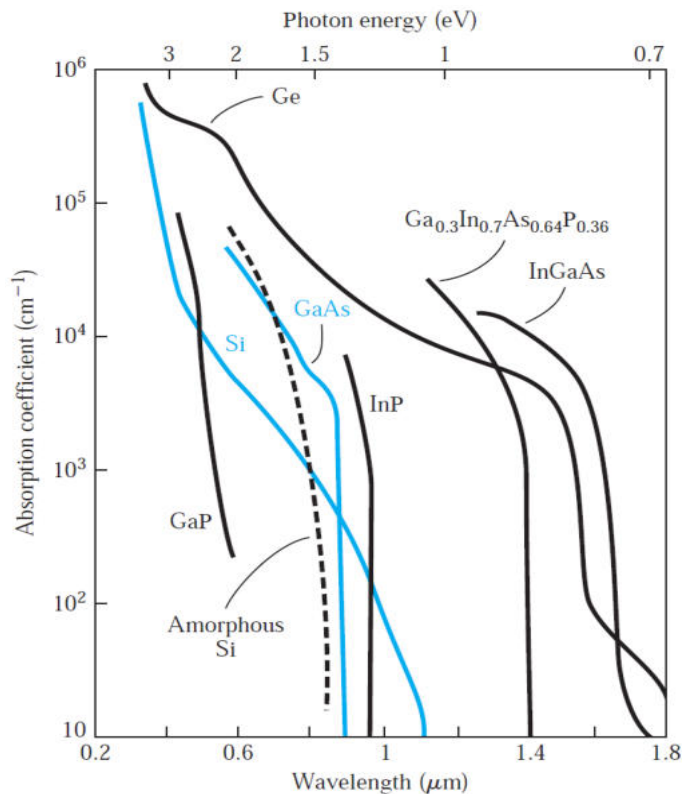


**Figure 3.27:** Absorption coefficient  $\alpha$  versus wavelength for some semiconductors.

and expressed in terms of energy  $\text{cm}^{-2}\text{s}^{-1}$ , decreases exponentially with distance  $x$  through the semiconductor material as

$$I_V(x) = I_V(0)e^{-\alpha x}. \quad (3.58)$$

This is shown in Fig. 3.26 as a function of  $x$  for two different values of the absorption coefficient  $\alpha$ , the relative number of photons absorbed per unit distance, given in units of  $\text{cm}^{-1}$ . If the absorption coefficient is large, all photons are absorbed over a relatively short distance. The absorption coefficient in the semiconductor is heavily dependent on the photon energy and bandgap energy, and on the nature of the bandgap. Indirect-bandgap semiconductors, like silicon, have much lower absorption than direct semiconductors, like most III-V semiconductors. This is illustrated in Fig. 3.27 where the absorption coefficient is plotted as a function of wavelength  $\lambda = c/\nu$  for several semiconductor materials. The absorption coefficient  $\alpha$  increases very rapidly for  $h\nu > E_g$ , or for  $\lambda (\mu\text{m}) < \frac{1.24}{E_g(\text{eV})}$ . The absorption becomes very small for  $h\nu < E_g$ , so the semiconductor appears transparent to photons in this energy range.

In addition to the interband processes in Fig. 3.25, absorption of light can also occur within a band (intraband process). It occurs in doped semiconductors and involves carriers that can move freely, such as electrons in the conduction band and/or holes in the valence band. This process is called free-carrier absorption (FCA, also called plasma effect) and plays a significant role in lowering the efficiency of light emission in semiconductor lasers (see Chapter 29). The optical power absorption coefficient  $\alpha_{FC}$  due to free carrier absorption is obtained as (see Numai[118], App. F).

*absorption coefficient*

*interband absorption intraband absorption plasma effect free-carrier absorption*

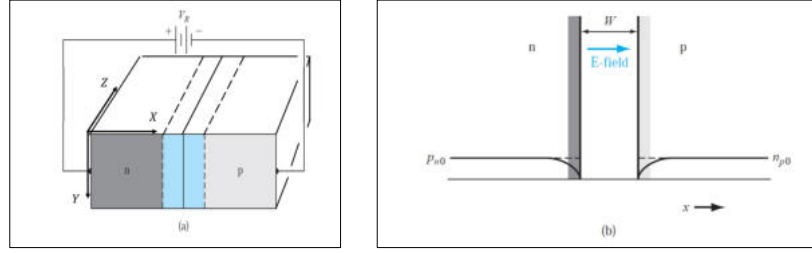


**Figure 3.28:** (a) Sketch of reverse-biased pn-junction. (b) Corresponding minority carrier concentrations

$$\alpha_{FC} = \frac{ne^2}{m^* \omega^2 \epsilon_0 n_\tau c \tau}, \quad (3.59)$$

where  $n$  is the carrier density,  $m^*$  the effective mass of the carrier,  $\omega$  the angular frequency of the light,  $\epsilon_0$  the permittivity in vacuum,  $n_\tau$  the refractive index,  $c$  the speed of light in vacuum and  $\tau$  the mean free time between carrier collisions.

### 3.7.2 Photodetectors

There are several semiconductor devices that can be used to detect the presence of photons. These devices are known as photodetectors; they convert optical signals into electrical signals. When excess electrons and holes are generated by the light in a semiconductor, there is an increase in the conductivity of the material. This change in conductivity is the basis of the photoconductor, perhaps the simplest type of photodetector. If electrons and holes are generated within the space charge region of a pn-junction, then they will be separated by the electric field and a current will be produced in the external circuit. The pn-junction is the basis of several photodetector devices including the photodiode and the phototransistor.

**pn-Photodiode** A pn-photodiode is a pn-junction diode operated with an applied reverse-bias voltage (Fig. 3.28(a)). We will consider a broad (i.e., in the x-direction) diode under reverse bias voltage, in which excess carriers are generated uniformly throughout the semiconductor device. Fig. 3.28(a) shows the reverse biased diode in an optical wave-guide configuration. Fig. 3.28(b) shows the minority carrier distribution in the reverse biased junction prior to photon illumination.

Under the influence of a flux  $\Phi(x, y, z)$  of photons propagating in the z-direction, excess carriers will be generated within the space charge region (blue area, width  $W_i$ , Fig. 3.28(a)). Then assuming each absorbed photon produces one electron and one hole, the generation rate of excess carriers is

$$G(x, y, z) = 2\alpha\Phi(x, y, z), \quad (3.60)$$

with  $\alpha$  the absorption coefficient (per unit of length). These excess carriers are swept out of the depletion region very quickly by the electric field, the electrons are swept into the n-region and the holes into the p-region.

The photon-generated current density from the space charge region is given by

$$J_i(y, z) = e \int_{W_i} dx G(x, y, z) = 2e\alpha \int_{W_i} dx \Phi(x, y, z), \quad (3.61)$$

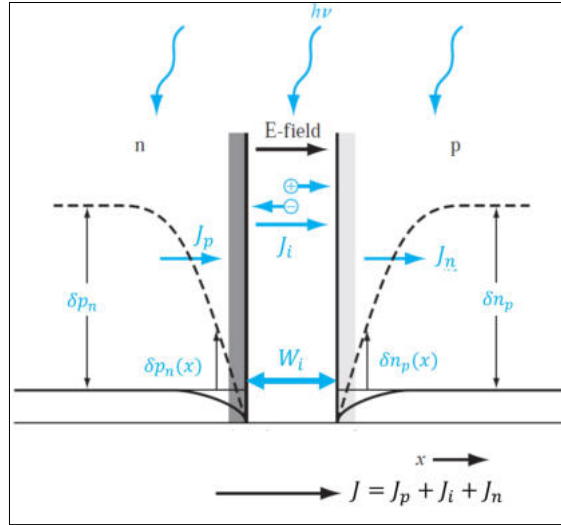


**Figure 3.29:** Steady-state, photo-induced minority carrier contributions  $\delta p_n, \delta n_p$  and photocurrents  $J_p, J_i, J_n$  in a broad reverse-biased pn-junction.

where the integral is over the space charge region width  $W_i$ . We may note that  $J_i$  is in the reverse-biased  $x$ -direction through the pn-junction. This photocurrent density responds very quickly to the photon illumination and is known as the prompt photocurrent. In fact, the speed of the photodiode is limited by the carrier transport through the space charge region, which can be estimated as follows. If we assume that the saturation drift velocity is  $10^7$  cm/s and the depletion width is  $2 \mu\text{m}$ , the transit time is  $\tau_t \sim 20$  ps. Hence, the cut-off frequency is  $f_{max} \sim 50$  GHz. This frequency response is substantially higher than that of photoconductors ( $\leq 1$  GHz). A photoconductor utilizes “across-the-gap” electron-hole pair creation and/or ionization of doped impurities in the material so as to exhibit light-induced conductivity.

There are two other, much slower, but larger, contributions to the photon-generated current density. These are due to excess carriers generated in the neutral n and p-regions of the diode. With these contributions the total steady-state diode photocurrent density for the broad diode is now

$$J(y, z) = 2e\alpha \sum_{j=i,n,p} \int_{W_j} dx \Phi(x, y, z), \quad (3.62)$$

where  $W_{n,p}$  are the diffusion lengths of the photo-induced minority carriers in the n, p-regions. Representative values are  $W_i \sim 1 \mu\text{m}$ ,  $W_n \sim 30 \mu\text{m}$ ,  $W_p \sim 10 \mu\text{m}$ . In most pn-junction structures, the assumption of a broad diode will not be valid, so modifications of the photocurrent expression 3.62 are possible.

The time response of the diffusion components of the photocurrent is relatively slow since these currents are the results of the diffusion of minority carriers toward the depletion region. The diffusion components of photocurrent are referred to as the delayed photocurrent. The photo-induced currents situation is schematically summarized in Fig. 3.29.

**PIN-photodiode** In many photodetector applications, the speed of response is important; therefore, the prompt photocurrent, generated in the space charge region, is

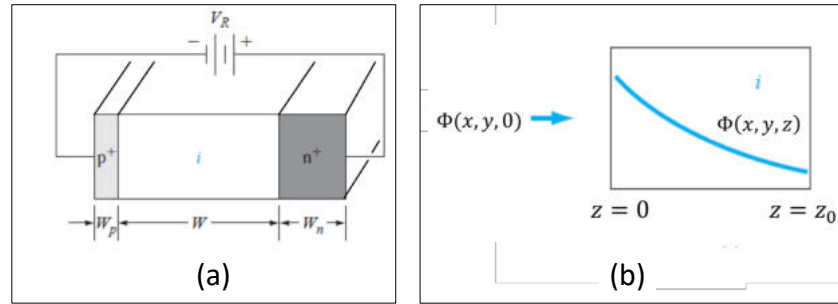


**Figure 3.30:** (a) A reverse-bias PIN photodiode. (b) Geometry showing nonuniform photon absorption.

the only photocurrent of interest. To increase the photodetector sensitivity, the depletion region width should be made as large as possible. This can be achieved in a PIN photodiode, which consists of a p-region and an n-region separated by an intrinsic region  $i$ . A sketch of a PIN diode is shown in Fig. 3.30a. The intrinsic region width  $W$  is much larger than the space charge width of a normal  $pn$ -junction. If a reverse bias is applied to the PIN diode, the space charge region extends completely through the intrinsic region.

Assume that a photon flux density  $\Phi(x, y, 0)$  in the  $z$ -direction is incident on the  $i$ -region. If we disregard the carrier generation in the  $p$  and  $n$ -regions, then the photon flux, as a function of distance, in the intrinsic region is  $\Phi(x, y, z) = \Phi(x, y, 0)e^{-\alpha z}$ , where  $\alpha$  is the photon absorption coefficient. This nonlinear photon absorption is shown in Fig. 3.30(b). The reverse biased photocurrent density generated in the intrinsic region is found as

$$J(y, z_0) = 2e\alpha \int_W dx \int_0^{z_0} dz \Phi(x, y, z) = 2e \int_W dx \Phi(x, y, 0)(1 - e^{-\alpha z_0}). \quad (3.63)$$

This equation assumes that there is no electron–hole recombination within the  $p$  and  $n$  regions and that each photon absorbed creates one electron–hole pair.

### 3.7.3 Light emission

In semiconductors, the transitions of electrons from high energy states to low energy states are designated recombinations of the electrons and the holes. We distinguish between radiative and nonradiative recombinations. A radiative recombination is accompanied by the emission of a photon whose energy corresponds to the energy difference between the initial and final states. In contrast, in a nonradiative recombination no photon is emitted, but the energy difference in the transition is transferred in a different way, e.g., by acoustic vibrations of the crystal lattice, called phonons or, more general, transformed into forms other than photons or phonons.

Let us now consider the transitions of electrons from the bottom of the conduction band down to the top of the valence band. If the bottom of the conduction band and the top of the valence band occur at the same wave vector  $\mathbf{k}_0$  (often  $\mathbf{k}_0 = 0$ ), this situation is referred to as a direct transition. A transition, in which the bottom of the conduction band and the top of the valence band have different  $\mathbf{k}$ -values, is referred to as indirect transition. These direct and indirect transitions are schematically shown in Fig. 3.31. Light emission due to radiative recombinations, also called luminescence,

*radiative recombination*  
*nonradiative recombination*  
*phonon*

*direct transition*

*indirect transition*  
*luminescence*

**Problem 3.8:** Depletion voltage of the active layer.

**Problem):** Estimate the voltage that is required to deplete the active layer of the reversely biased SOA-structure, for use as a detector. What is the effect if it is not completely depleted?

**Solution):** Complete depletion means the depletion width has to be larger than the active layer thickness. For the standard SOA structure,  $W_{\text{active}} = 500$  nm. If the Q1.25 is truly intrinsic, the active layer should already be depleted at equilibrium (0 V). In practice, background doping always exists. Let's assume an n-doping of  $10^{16}$ , and calculate the voltage needed to deplete that at  $T = 300$  K. The p-n junction between InP and Q1.25 is a heterojunction, and therefore, band offsets must be considered. From [119] we know:  $\Delta E_c \approx 2\Delta E_v$ . From Problem 3.2, we know that Q1.25 corresponds to  $\text{Ga}_x\text{In}_{1-x}\text{As}_y\text{P}_{1-y}$  with  $y \approx 0.689$ ,  $x = 0.47y \approx 0.324$ ,  $E_g \approx 0.99$  eV. Hence  $\Delta E_v \approx \frac{1.344-0.99}{3} = 0.118$  eV,  $\Delta E_c \approx 2 \times \frac{1.344-0.99}{3} = 0.236$  eV. Since the built-in potential is equal to the difference between the Fermi levels of isolated semiconductors, it can be similarly calculated with the following equation:

$$eV_b = \frac{\Delta E_c - \Delta E_v}{2} + k_B T \ln \frac{N_d N_a}{n_{i,p} n_{i,n}} + \frac{k_B T}{2} \ln \frac{N_{v,n} N_{c,p}}{N_{c,n} N_{v,p}}.$$

From Problem 3.3, we know that

$$N_{c,n} \approx 3.1 \times 10^{17} \text{ cm}^{-3}, N_{v,n} \approx 8.2 \times 10^{18} \text{ cm}^{-3}, N_{c,p} \approx 5.7 \times 10^{17} \text{ cm}^{-3},$$

$$N_{v,p} \approx 1.1 \times 10^{19} \text{ cm}^{-3}, n_{i,n} \approx \sqrt{5.86 \times 10^{19}} \approx 7.66 \times 10^9 \text{ cm}^{-3}.$$

$$n_{i,p} \approx \sqrt{1.65 \times 10^{14}} \approx 1.28 \times 10^7 \text{ cm}^{-3}. V_b \text{ can then be calculated: } V_b \approx 1.04 \text{ V.}$$

Similar to the deduction for homojunctions and using charge neutrality, the depletion length in InGaAsP can be expressed as:

$$x_n = \sqrt{\frac{2\epsilon_p \epsilon_n \epsilon_0}{e} \frac{N_a}{N_d(\epsilon_p N_a + \epsilon_n N_d)}} (V_b + V_R) = 500 \text{ nm. From [102] we have}$$

$\epsilon_n = 12.5 + 1.44y \approx 13.5$ ,  $\epsilon_p = 12.5$ . Solving the equation produces  $V_R \approx 2.43$  V. If the junction is not fully depleted, then the detector becomes slower, because diffusion still has a large effect, and carrier diffusion is much slower than drift.

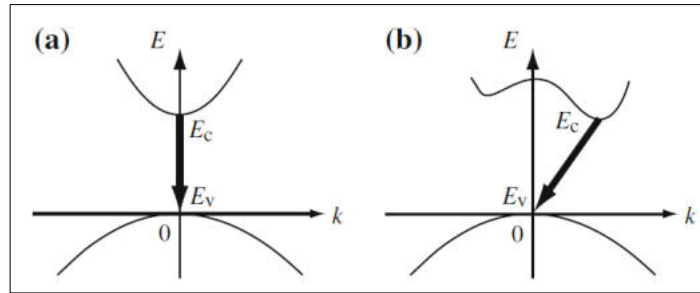


**Figure 3.31:** Direct (a) and indirect (b) transitions.

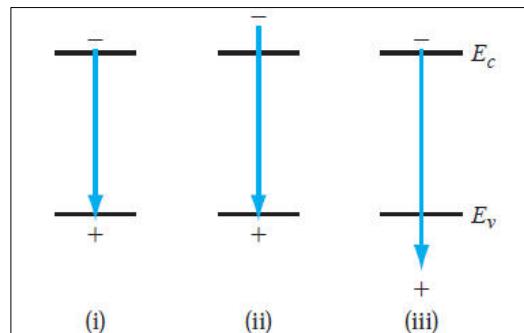


**Figure 3.32:** (a) The basic interband transitions: (i) intrinsic emission with energy close to the bandgap energy, (ii) emission from energetic electron and (iii) emission to energetic hole.

is only possible for direct transitions. The reason is conservation of momentum and since a photon carries a negligible amount of momentum, this implies equal momentum for the initial and final states, or  $\Delta k \approx 0$ . Indirect transitions, on the other hand, need emission of a momentum-carrying phonon.

Some recombination processes may result in photon emission from direct bandgap materials. If a recombination occurs with the emission of a photon, one refers to *spontaneous emission* in case the electron hole pair was formed by thermal excitation or luminescence when the pair is formed by other means, such as electrical (electroluminescence) or optical (photoluminescence). Figure 3.32 shows the basic *interband transitions*, where case (i) corresponds to an intrinsic emission very close to the bandgap energy of the material. Cases (ii) and (iii) correspond to energetic electrons or holes. If either of these recombinations result in the emission of a photon, the energy of the emitted photon will be slightly larger than the bandgap energy. There will then be an *emission spectrum* and a bandwidth associated with the emission (See Fig. 3.35).

The possible recombination processes involving impurity or defect states are shown in Figure 3.33. Case (i) is the conduction band to acceptor transition, case (ii) the donor to valence-band transition, case (iii) the donor to acceptor transition, and case (iv) is the recombination due to a deep trap. Case (iv) is a non-radiative process; the other recombination processes may or may not result in the emission of a photon. Figure 3.34 shows the *Auger recombination* process, which can become important in direct bandgap materials with high doping concentrations. The Auger recombination process is a nonradiative process. In case (i), it is a recombination between an electron

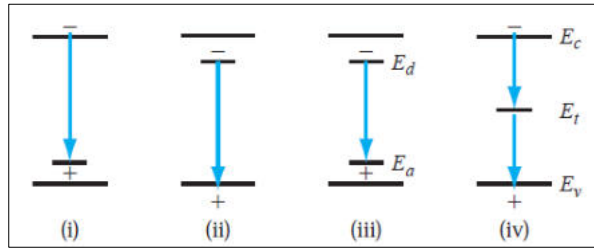


**Figure 3.33:** Recombination processes involving impurity or defect states: (i) conduction band to acceptor, (ii) the donor to valence-band transition, case (iii) the donor to acceptor transition, and case (iv) is the recombination due to a deep trap. Case (iv) is a non-radiative process.

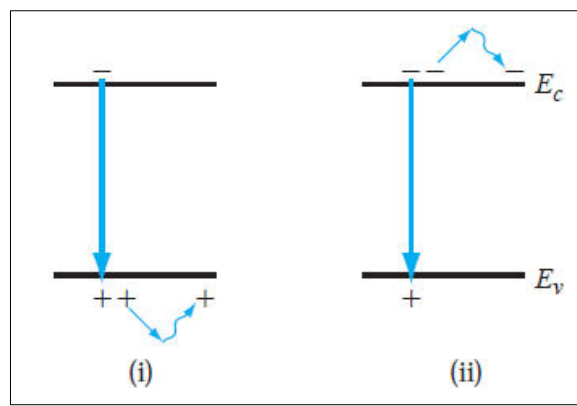


**Figure 3.34:** The Auger recombination process (nonradiative): (i), recombination between an electron and hole, accompanied by the transfer of energy to another free hole, (ii) recombination between an electron and hole with transfer of energy to a free electron.

and a hole, accompanied by the transfer of energy to another free hole. Similarly, in case (ii), the recombination between an electron and hole results in the transfer of energy to a free electron. The third particle involved in this process will eventually lose its energy to the lattice in the form of heat. The process involving two holes and an electron would occur predominantly in heavily doped p-type materials, and the process involving two electrons and a hole would occur primarily in a heavily doped n-type material.

As argued around Fig. 3.32, the emission of a photon is not necessarily at a single, discrete energy, but can occur over a range of energies. The spontaneous emission rate generally has the form (71)

$$I(\nu) \propto \nu^2 (\hbar\nu - E_g)^{\frac{1}{2}} e^{-\frac{\hbar\nu - E_g}{k_B T}}, \tag{3.64}$$

where  $E_g$  is the bandgap energy. Figure 3.35 shows the emission spectra from gallium arsenide.

**Luminescent efficiency** We have shown that not all recombination processes are radiative. An efficient luminescent material is one in which radiative transitions predominate. The quantum efficiency  $\eta_q$  is defined as the ratio of the radiative recombination *quantum efficiency*

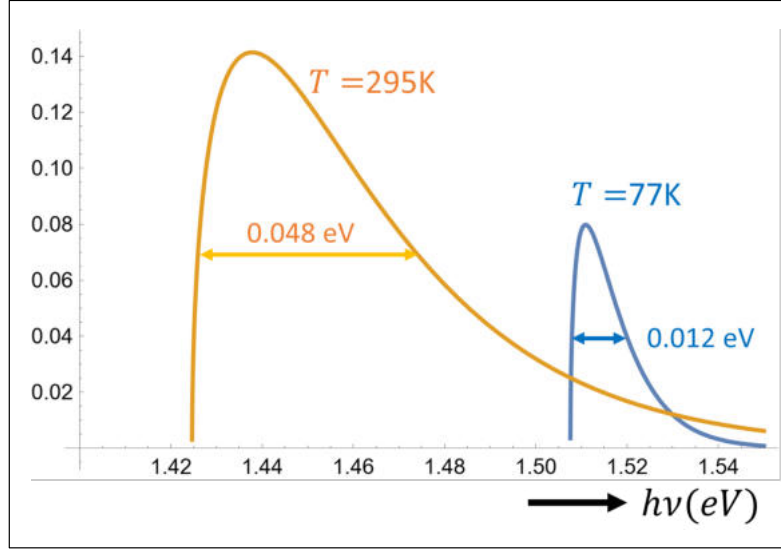


**Figure 3.35:** GaAs diode emission spectra at  $T = 300\text{ K}$  and  $T = 77\text{ K}$ . (calculated from Eq. 3.64)

rate to the total recombination rate for all processes, or

$$\eta_q = R_r / R, \quad (3.65)$$

*radiative recombination rate lifetime* with  $R_r$  the radiative recombination rate and  $R$  the total recombination rate of the excess carriers. Since the recombination rate is inversely proportional to lifetime, we can write the quantum efficiency in terms of lifetimes as

$$\eta_q = \frac{\tau_{nr}}{\tau_r + \tau_{nr}}, \quad (3.66)$$

where  $\tau_{nr}$  is the nonradiative lifetime and  $\tau_r$  is the radiative lifetime. For a high luminescent efficiency, the nonradiative lifetime must be large; i.e., the probability of a nonradiative recombination is small compared to the radiative recombination. The interband recombination rate of electrons and holes is directly proportional to the number of electrons available and directly proportional to the number of available empty states (holes). We can write

$$R_r = Bnp, \quad (3.67)$$

where  $R_r$  is the band-to-band radiative recombination rate and  $B$  is the constant of proportionality. The values of  $B$  for direct-bandgap materials are on the order of 100 times larger than for indirect bandgap materials. The probability of a direct band-to-band radiative recombination transition in an indirect bandgap material is very unlikely.

## 3.8 Stimulated emission and amplification

### 3.8.1 Stimulated emission

Suppose an electron occupies a state in the conduction band, while a hole in the valence band is present with the same momentum  $\mathbf{k}$ . If the electron recombines with the

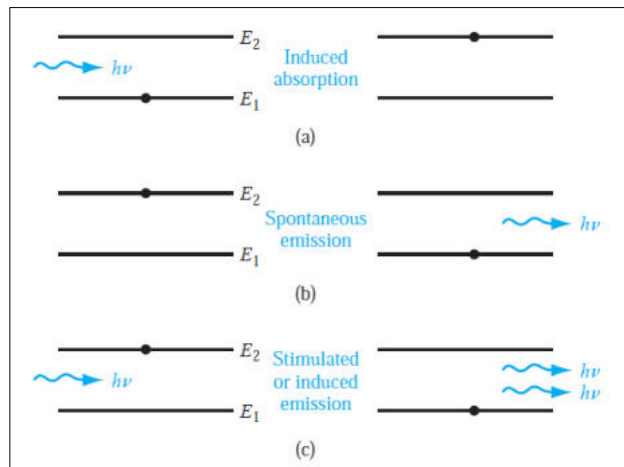


**Figure 3.36:** Schematic diagram showing (a) induced absorption, (b) spontaneous emission, and (c) stimulated emission processes.

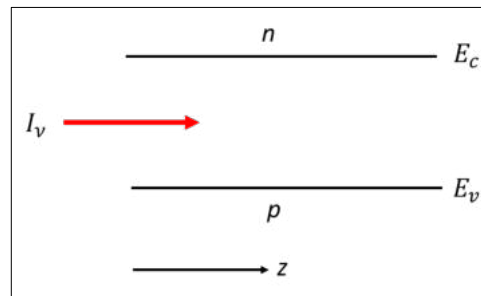


**Figure 3.37:** Light propagating in the  $z$ -direction through a material with conduction and valence bands.

hole without any external trigger, a photon will be emitted. This is *spontaneous emission*, discussed in the previous section. However, if an incident photon with nearly the same energy as the transition triggers the transition, we end up with two identical photons. This is *stimulated emission*, a process that can be fully understood by quantum theory. Stimulated emission leads to amplification of the light, preserving the optical phase. Fig. 3.36 illustrates the basic processes of induced absorption, spontaneous emission, and stimulated emission.

Now, consider propagation of light in a material with density  $n_c$  of electrons in the conduction band and density  $n_v$  of electrons in the valence band, as illustrated in Fig. 3.37.

In case that  $n_c > n_v$ , there will be more stimulated emissions than absorptions, that is, the intensity will increase on propagation, or, equivalently, the beam is amplified. The change in intensity as a function of  $z$  can be written as

$$\frac{dI}{dz} = \sigma_i(n_c - n_v)I, \quad (3.68)$$

where  $\sigma_i$  is the cross section for an incident photon to induce a transition. It is noted that  $\sigma_i$  depends on the frequency of the light and has the dimension of an area (length

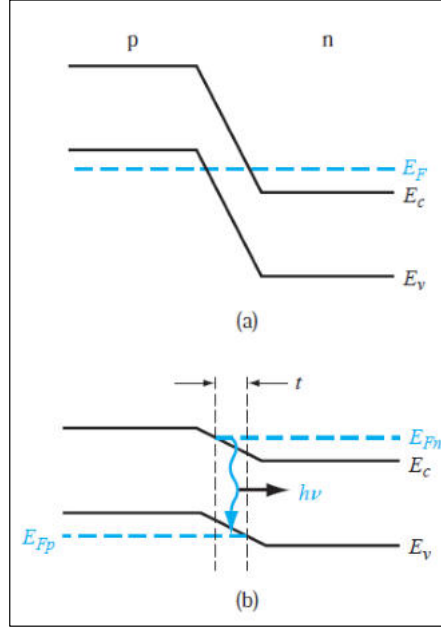


**Figure 3.38:** (a) Degenerately doped pn-junction at zero bias. (b) Degenerately doped pn-junction under forward bias with photon emission.

× length). In this equation we assume no loss mechanisms and disregard the spontaneous emission. The solution of Eq. 3.68 can be written as

$$I(z) = I(0)e^{gz}, \quad (3.69)$$

where  $g \equiv \sigma_i(n_c - n_v)$  is the net amplification or gain factor. Amplification occurs when  $g > 0$  and absorption when  $g < 0$ . Hence, amplification is obtained when  $n_c > n_v$ , a situation called population inversion, which can be realized in a forward-biased pn-junction diode, if both sides of the junction are degenerately doped (see Sec. 3.4). Figure 3.38(a) shows the energy-band diagram of such a junction in thermal equilibrium. The Fermi level is in the conduction band in the n-region and in the valence band in the p-region.

Figure 3.38(b) shows the energy bands of the pn-junction when the forward bias is applied. We see that in the depletion region a situation is realized where electrons and holes are both present. There are large numbers of electrons in the conduction band directly above many holes. These electrons and holes can recombine under emission of a photon with energy  $E_g < h\nu \leq E_{Fn} - E_{Fp} = eV_a$ , where  $V_a$  is the applied (forward) voltage. A more elaborate analysis taking account of the density of states in the conduction and valence bands yields that the gain factor is given by

$$g(\nu) = \sigma_i(n_c - n_v) \propto \sqrt{h\nu - E_g} \left\{ 1 - e^{-\frac{h\nu + E_{Fp} - E_{Fn}}{k_B T}} \right\}. \quad (3.70)$$

For  $g(\nu) > 0$ , we must have  $h\nu > E_{Fn} - E_{Fp}$ , which implies that the junction must be degenerately doped since we also have the requirement that  $h\nu \geq E_g$ . Near the junction, there is a region in which the population inversion occurs. Under these above-mentioned conditions, the pn-junction serves as an amplifier for light, a Semiconductor Optical Amplifier (SOA).

### 3.9 Heterostructures and Double Heterojunction

In the previous section we have considered a homojunction between two sections of the same semiconductor crystal. We will now study a junction between two not necessarily equal semiconductors that have opposite type of doping. This is referred to as a heterojunction. Figure 3.39 shows a schematic picture of a heterostructure. The left figure shows a heterojunction of a p-type semiconductor with a n-type semiconductor whereby  $E_g$  is the largest in the n-area. A similar band-bending occurs as in the pn-homojunction (see Fig. 3.17). At the boundary plane, however, a discontinuity occurs. In the figure the situation for forward bias is depicted, where we have left the bandbending behind.

In a regular forward biased pn-junction, there is an electron as well as a hole current through the junction. The relative magnitude of these two currents is determined by the relative doping levels. In a heterojunction the current will mainly consist of charges coming out of the material with the highest bandgap into the one with the lowest bandgap, independent of the doping.

A very important structure is the double heterojunction (DH) in which a layer with a low bandgap is placed between two layers with a large bandgap. On the right in Fig. 3.39 the basic band diagram of a double heterojunction is depicted. Such a structure forms a potential well for the electrons and the holes and, therefore, the concentration of carriers can be much higher than in a homojunction. Most of the semiconductor lasers are based on the charge confinement in such a potential well. When forward biased, electrons are brought out of the n-area and holes out of the p-area. The lower-bandgap layer is usually undoped (non-intentionally doped). The confinement of a large electron and hole density in the p-layer leads to population inversion and the recombination results in laser emission. Furthermore, the material with a lower bandgap usually has a higher refractive index. The structure thus acts as a waveguide in which the photons are trapped by total internal reflection. Such a double heterostructure thus combines carrier confinement with optical (photon) confinement, which provides it with a large interaction between photons and carriers, leading to both a large gain in forward bias.

---

This section is largely copied from the syllabus Photonics by Roel Baets and Günther Roelkens from the Photonics Research Group (Ghent University).

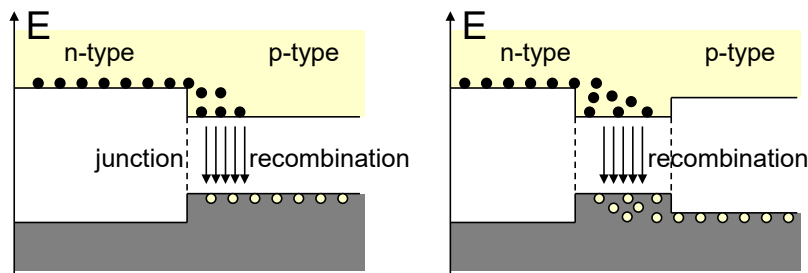


**Figure 3.39:** Schematic diagram of a heterojunction and a double heterojunction.

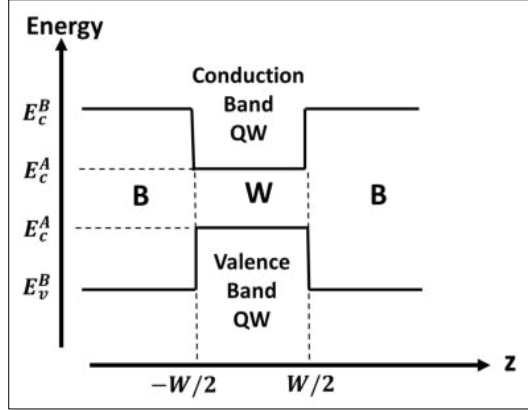


**Figure 3.40:** Schematic of the conduction and valence band-edge function  $E_n^{edge}(z)$  for a Type I double heterostructure quantum well (QW). **B** stands for barrier material and **W** for well material.

### 3.10 Quantum-well double heterostructures

We will now study a situation where a direct-bandgap semiconductor **W** (the “well” material), is sandwiched between a semiconductor **B** (the “barrier” material) at both sides, where the bandgap energies satisfy  $E_g^W < E_g^B$ , and the respective conduction and valence band edges  $E_c^W, E_v^W$  and  $E_c^B, E_v^B$  connect as sketched in Fig. 3.40. Such a band-edge situation is referred to as Type I line up. Well/Barrier combinations such as GaAs/AlGaAs, InGaAs/InP and GaN/AlGaIn all have type I line up. Once the band line up is known, one has to decide how the electronic states in the heterostructure should be described. An approach that has been quite successfully applied to heterostructures is, in its simplest form, the replacement of the original Schrödinger equation (see Eq. 3.3:

$$\left[ -\frac{\hbar^2}{2m} \nabla^2 + U_c(\mathbf{r}) \right] \psi_{n,k}(\mathbf{r}) = E_n(\mathbf{k}) \psi_{n,k}(\mathbf{r})$$

by

$$\left[ -\frac{\hbar^2}{2m_n} \nabla^2 + E_n^{edge}(z) \right] \Phi_n(\mathbf{r}) = E \Phi_n(\mathbf{r}) \quad (3.71)$$

where the crystal potential  $U_c(r)$  is replaced by the band-edge energy  $E_n^{edge}(z)$  with  $n$  indicating the conduction ( $n = c$ ) or valence band ( $n = v$ ), while the effect of the background potential is contained in the corresponding effective mass  $m_n$ . In the simple approximation of Eq. 3.71), the Schrödinger equation for the electron states in the conduction-band quantum well can be written

$$\left[ -\frac{\hbar^2}{2m_c} \nabla^2 + V(z) \right] \Phi(\mathbf{r}) = E \Phi(\mathbf{r}), \quad V(z) = \begin{cases} 0 & , |z| \leq \frac{W}{2} \\ E_c^B - E_c^W & , |z| > \frac{W}{2} \end{cases} \quad (3.72)$$

Since the potential  $V$  depends only on  $z$ , the wave function  $\Phi(\mathbf{r})$  can be separated as follows:

$$\Phi(\mathbf{r}) = e^{ik_x x} e^{ik_y y} f(z), \quad (3.73)$$

where  $f(z)$  satisfies the 1D Schrödinger equation

$$\left[ -\frac{\hbar^2}{2m_c} \frac{d^2}{dz^2} + V(z) \right] f(z) = E f(z) \quad (3.74)$$

and the total energy  $E$  is given by

$$E = \frac{\hbar^2}{2m_c} (k_x^2 + k_y^2) + E_n. \quad (3.75)$$

Hence, each level  $E_n$  defines a parabolic subband in the  $x, y$  plane. Assuming the barrier infinitely high, the wavefunction solutions are confined to the well. In that case, the corresponding electron is confined to the well, but can move freely in the  $x, y$  plane with effective mass  $m_c$ . The wave functions  $f(z)$  are given by

$$f(z) = \begin{cases} \cos\left(\frac{\pi n z}{W}\right) & , \quad n = 1, 3, 5, \dots \\ \sin\left(\frac{\pi n z}{W}\right) & , \quad n = 2, 4, 6, \dots \end{cases}, \quad (3.76)$$

with the corresponding well energies

$$E_n = \frac{\hbar^2}{2m_c} \frac{\pi^2 n^2}{W^2}. \quad (3.77)$$

If the barrier potential is not infinite, only the energy levels that satisfy  $E_n < E_c^B - E_c^W$  correspond to electrons bound to the well, but with exponentially decaying wavefunction tails in the barrier regions. This is schematically indicated in Fig. 3.41.

In Sec. 3.3, we derived the number of electron states with energy between  $E$  and  $E + dE$  (see Eq. 3.12) as  $N_c(E)dE = \frac{2V_c}{(2\pi)^2} \left(\frac{2m_c}{\hbar^2}\right)^{3/2} (E - E_c)^{1/2} dE$ . In the quantum-well situation, however, this number is different and can be derived following a similar reasoning as in the derivation of Eq. 3.12, but now for each quantum level  $n$  the 2-dimensional parabola given by Eq. 3.75 must be considered. Thus the number of electron states in the conduction band with energy between  $E$  and  $E + dE$  is given by the number of  $k$ -points in the circle band with radius  $k = \sqrt{2m_c(E - E_c^W - E_n)}/\hbar$  and thickness  $dk$ , or  $N_n(E)dE = \frac{2V_c}{(2\pi)^2 W} 2\pi k \frac{dk}{dE} dE$ , with  $W$  the QW width. Hence, substituting for  $k$  and performing the differentiation, we obtain

$$N_n(E)dE = \begin{cases} \frac{V_c m_c}{\pi \hbar^2 W} dE & , \quad E > E_c^W + E_n \\ 0 & , \quad E < E_c^W + E_n \end{cases}, \quad n = 1, 2, \dots \quad (3.78)$$

Thus for each quantum number  $n$ , the density of states per unit volume is constant when  $E > E_c^W + E_n$ . The overall density of states is the sum of the densities for all values of  $n$ , so that it exhibits the staircase distribution shown in Fig. 3.42. Each step of the staircase corresponds to a different quantum number  $n$  and may be regarded as a subband within the conduction band. The bottoms of these subbands move progressively higher for higher quantum numbers. It is easily shown by substituting  $E = E_c^W + E_n$  in Eq. 3.12, and by using Eq. 3.78, that at  $E = E_c^W + E_n$ , the quantum-well density of states is the same as that for the bulk. The density of states in the valence band has a similar staircase distribution. In contrast with bulk semiconductor, the quantum-well structure exhibits a substantial density of states at its lowest allowed conduction-band energy level and at its highest allowed valence-band energy level.

### 3.11 Quantum Dots

Quantum dots (QDs) are tiny semiconductor structures with a very small size in each of the three dimensions. They can e.g. be of spherical shape as for instance the colloidal

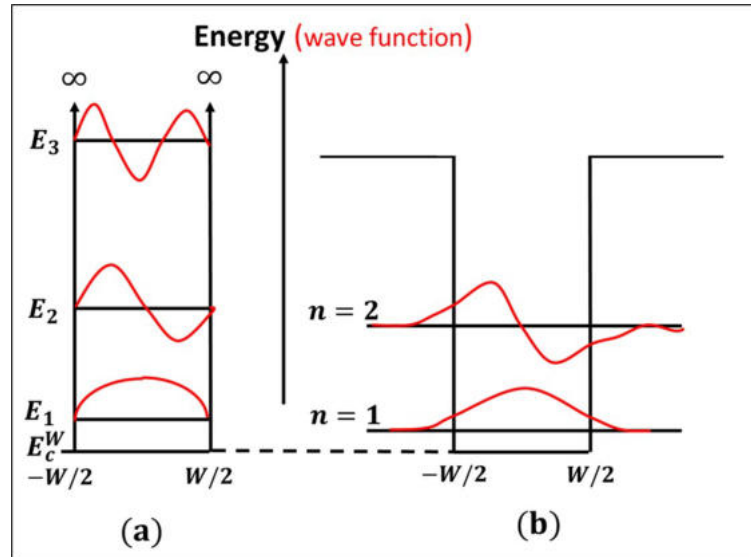


**Figure 3.41:** Schematic picture of the conduction-band QW energy levels comparing infinite (a) and finite (b) barriers. In case (b), only a finite number of confined states exists.

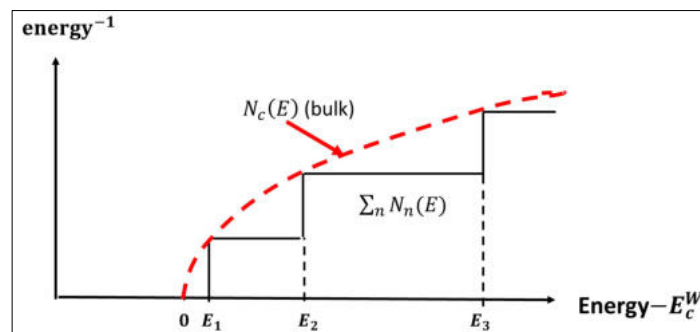


**Figure 3.42:** Schematic of density of states in a one-dimensional quantum well.

nanocrystals used for QD displays. Their shape can be chosen arbitrarily, provided that quantum confinement (see Fig. 3.40) is present in all three directions. For simplicity, we will start to describe a cubic QD. A cubic quantum dot can be viewed as a quantum well in each direction with length  $L_x$ ,  $L_y$ ,  $L_z$ . Similar to a quantum well (Eq. 3.77), the confinement energy for the electrons and the heavy holes in a QD becomes

$$E_{l,m,n}^{electron} = \frac{\pi^2 \hbar^2}{2m_e^*} \left( \frac{l^2}{L_x^2} + \frac{m^2}{L_y^2} + \frac{n^2}{L_z^2} \right) \quad (3.79)$$

$$E_{l,m,n}^{heavy-hole} = \frac{\pi^2 \hbar^2}{2m_{hh}^*} \left( \frac{l^2}{L_x^2} + \frac{m^2}{L_y^2} + \frac{n^2}{L_z^2} \right), \quad (3.80)$$

in which  $m_e^*$  and  $m_{hh}^*$  are the electron and heavy-hole effective masses, and  $l$ ,  $m$ ,  $n$  are integer (1, 2, ...) quantum numbers. Note that we assume here a simple unstrained QD in which the heavy-hole band is the uppermost valence band. For the simplest case in which  $L_x = L_y = L_z$ , the ground state can be labeled as  $(l,m,n) = (1,1,1)$  and might contain up to 2 electrons (or holes) due to the spin degeneracy, which implies that the ground state level can be occupied by 1 spin-up electron and 1 spin-down electron. The maximum number of electrons in the ground state level of the conduction band (or holes in the valence band ground state) is limited to two due to the Pauli exclusion principle of quantum mechanics. The first excited state level is 6 times degenerate and is denoted as the  $(2,1,1)$ ,  $(1,2,1)$  or  $(1,1,2)$  level, each with spin degeneracy 2.

For a semiconductor optical amplifier (SOA), the optical gain is proportional to the joint density of states, which is the combined density of states for the conduction and the valence band. It can be derived that the expression for the joint density of states is exactly the same as for the conduction band density of states, provided that the effective electron mass  $m_e^*$  is replaced by the reduced effective mass  $\mu$ , which is given by  $\frac{1}{\mu} = \frac{1}{m_e^*} + \frac{1}{m_{hh}^*}$ . The joint density of states,  $J_\alpha(\epsilon)$ , in a semiconductor with dimension  $\alpha$  can be expressed as ( $\epsilon = E - E_c$  or  $E_v - E$ )

$$J_3(\epsilon) = \frac{1}{2\pi^2} \left( \frac{2\mu}{\hbar^2} \right)^{3/2} \sqrt{\epsilon} \quad \text{Bulk semiconductor (3D), compare Eq.3.12}$$

$$J_2(\epsilon) = \frac{\mu}{\pi \hbar^2} \quad \text{Quantum Well (2D), compare Eq. 3.78}$$

$$J_1(\epsilon) = \frac{\sqrt{2\mu}}{\pi \hbar} \frac{1}{\sqrt{\epsilon}} \quad \text{Quantum Wire (1D)}$$

$$J_0(\epsilon) = \delta(\epsilon - \epsilon_0) \quad \text{Quantum Dot (0D)}$$

where the joint density of states for a quantum dot is a delta function, providing an infinitely large gain exactly at resonance ( $E_g + E_{1,1,1}^{electron} + E_{1,1,1}^{heavy-hole} = \epsilon_0$ ) between the electron and hole confinement levels, with  $E_g$  the bandgap of the QD material. In practice however, every QD has a slightly different size  $L_x$ ,  $L_y$ ,  $L_z$ . The inhomogeneous size distribution of the QDs thus provides a broadband gain spectrum with a peak gain of the same order of magnitude as for a conventional bulk semiconductor. Since the density of states is a delta-function, the same amount of optical gain is in principle available for small-size quantum dots as for large size quantum dots, thus providing a broadband gain spectrum. The peak gain can be optimized by using a high QD density and increasing the number of QD layers within the InP/InGaAsP separate confinement structure.

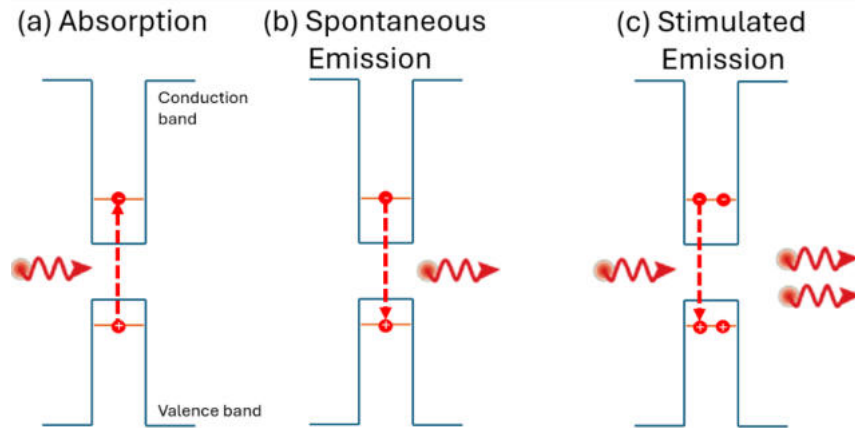


**Figure 3.43:** Optical gain in a semiconductor quantum dot, showing (a) optical absorption of a photon by creating an electron-hole pair, (b) spontaneous emission by the recombination of an electron and a hole, emitting a photon and, (c) stimulated emission in which an incoming photon at the left is creating an identical second photon in a population inverted QD.

A semiconductor quantum dot is able to absorb a photon, thus creating an electron-hole pair, as schematically depicted in Fig. 3.43 for resonant excitation. Once the QD is optically excited, it contains a single electron-hole pair which will spontaneously recombine with a lifetime of approximately 1 nanosecond by emitting a photon as shown in Fig. 3.43b. Stimulated emission resembles an absorption process, but it is a “reversed absorption process” in which an electron recombines with a hole by creating a second photon with identical wavelength and identical propagation direction as the incoming photon, as shown in Fig. 3.43c. For achieving stimulated emission, it is a necessary condition that the QDs are population inverted, which means that the excited state (i.e. the QD confinement level in the conduction band) is stronger populated (with electrons) than the ground state (i.e. the QD confinement level in the valence band). For the ground state level, this implies that the QD level in the conduction band is populated with 2 electrons and that the ground state level in the valence band is populated with two holes (2 missing electrons).

For the fabrication of a semiconductor optical amplifier, one usually employs self-assembled quantum dots (SAQDs). SAQDs are grown by the Stranski-Krastanov growth mechanism in which one grows InAs on InGaAsP that is lattice-matched to an InP substrate. Since the lattice constant of InAs is considerably larger than the lattice constant of InGaAsP (Fig. 3.44), the lattice constant of the InAs layer  $a_{||}$ , has to adapt to the smaller lattice constant of InGaAsP, causing a strong compression  $\frac{\Delta a}{a} = 0.032$  (3.2%) of the InAs layer. Since the compression of a semiconductor crystal with 3.2% requires an enormous amount of force, it is only possible to grow 4-5 heavily strained monolayers of InAs on InGaAsP as shown in Fig. 3.44b. Since the growth of an even thicker InAs layer would require an excessive amount of force, a kind of “droplet or island formation” appears in which InAs islands start to appear as shown in Fig. 3.44c. The island formation is energetically very favorable since the InAs lattice relaxes to its equilibrium lattice constant within the island. The self-assembled droplet formation thus relaxes the amount of force needed to compress the InAs layer, since now only the wetting layer needs to be compressed. These islands are sufficiently small to act as true quantum dots. Fig. 3.44d shows a scanning tunneling microscopy image of an InAs/GaAs

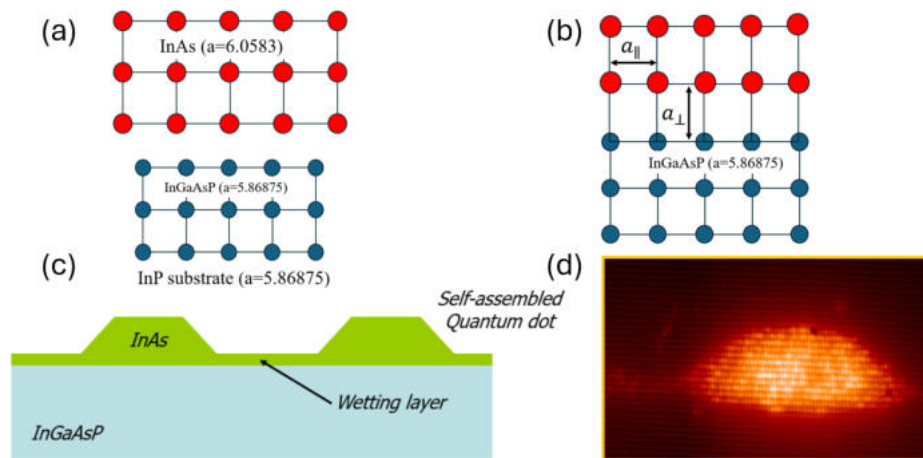


**Figure 3.44:** (a) InAs has a larger lattice constant than InGaAsP that is lattice matched to an InP substrate, thus preventing lattice matched growth. (b) The InAs wetting layer on InGaAsP is heavily compressively strained. (c) InAs self-assembled QDs spontaneously grow since it allows to reduce the strain. (d) Scanning Tunneling Microscopy (STM) image of an InAs self-assembled quantum dot 30 nm x15 nm on GaAs. Courtesy of P.M. Koenraad.

self assembled QD.

Although Fig. 3.43 is suggesting that population inverted QDs provide stimulated emission, the population inversion is immediately destroyed after each stimulated emission event. It is thus required that each QD is immediately “refilled” with a new electron-hole pair. This process is called “gain recovery”. In semiconductor physics, this refilling usually occurs by electron-phonon scattering, but this process is energetically forbidden for QDs since the optical phonon energy is generally not exactly equal to the splitting between the confined energy levels within the QD. It should be stressed that the wetting layer, which is a 2-dimensional quantum well, is an essential ingredient for the performance of a semiconductor optical amplifier. Although one usually draws the energy levels of a quantum wells as discrete energy levels, these confined energy states are only confined states in the growth direction, while conventional energy bands appear in the direction along the quantum well plane. The energy bands in the wetting layer feature a staircase-like continuous joint density of states, compare Fig. 3.42. For this reason, ultrafast gain recovery still happens on the order of a few picoseconds due to fast carrier-carrier scattering between electrons in the discrete QD levels and electrons within the continuous density of states of the 2D wetting layer, as schematically shown in Fig. 3.45 [120],[121],[122].

### 3.12 Excitons and Quantum confined Stark effect

The absorption of a photon can result in the formation of an electron and a hole at some distance from each other but which are nevertheless bound together by their mutual Coulomb interaction. This entity, which is much like a hydrogen atom but with a hole rather than a proton, is called an exciton. A photon may be emitted as a result of the electron and hole recombining, thereby annihilating the exciton.

In Sec. 3.3 the quantized wave vector  $\mathbf{k}$  was introduced such that  $\hbar\mathbf{k}$  is the quantized

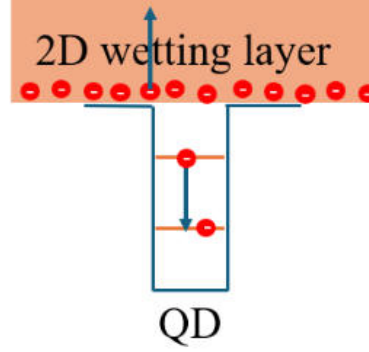


**Figure 3.45:** Gain recovery in a self-assembled Quantum Dot by carrier-carrier scattering between the discrete QD levels and the 2-dimensional wetting layer which has a continuous density of states. The blue arrows show an example of a carrier-carrier scattering process in which an electron in the excited QD state is scattered in to the QD ground state by obeying energy and momentum conservation during the scattering process.

crystal momentum. This was a consequence of the periodic crystal potential experienced by each individual independent electron. However, the electron and hole pair, including their Coulomb interaction, experience the crystal periodicity. Therefore, the exciton does, and we must replace  $\hbar\mathbf{k}$  by  $\hbar\mathbf{K}_{ex}$ , where  $\mathbf{K}_{ex} \equiv \mathbf{k}_c - \mathbf{k}_v$  is the quantized wave vector for the exciton (see Singh [123] and Dresselhaus [124]).

Then, in the approximation where the exciton is described as an electron in the central Coulomb field of a hole, the exciton energy levels are given by

$$E_n^{ex}(\mathbf{K}_{ex}) = E_g + E_n + \frac{\hbar^2}{2(m_c + m_v)} K_{ex}^2, \quad (3.81)$$

where  $E_g$  is the gap energy of the semiconductor and the exciton levels are given by

$$E_n = -R_{ex}/n^2 \equiv -\frac{m_r e^4}{2(4\pi\epsilon)^2 \hbar^2} \frac{1}{n^2}, \quad (3.82)$$

with  $m_r = \frac{m_e m_v}{m_c + m_v}$  the reduced effective mass of the electron-hole system and  $R_{ex} = \frac{m_r e^4}{2(4\pi\epsilon)^2 \hbar^2}$  the binding energy of the exciton. The last term in the right-hand side of 3.81 represents the kinetic energy of the exciton. The corresponding “Bohr radius”, i.e., the effective extent of the exciton can be expressed as

$$a_{ex} = \frac{\epsilon m_0}{\epsilon_0 m_r} a_B \quad (a_B = \text{Bohr radius} = 0.529 \times 10^{-10} \text{m}), \quad (3.83)$$

where  $m_0$  is the free-electron mass. The exciton radius is  $\sim 1 \times 10^{-8}$  m (see Table 1). Thus the exciton is spread over a large number of unit cells. A sketch of the exciton band structure situation is presented in Fig. 3.46.

Since a photon carries only a negligible amount of momentum, optical transitions from the valence band to an excitonic state can occur only at  $\mathbf{K}_{ex} \approx 0$ . Excitonic effects have very dramatic consequences for the optical properties of semiconductors, especially near the band edges. Below the band edge, there is a strong and sharp excitonic absorption/emission transition. Also just above the bandgap, there is a strong enhancement of the absorption process especially in 3D systems.

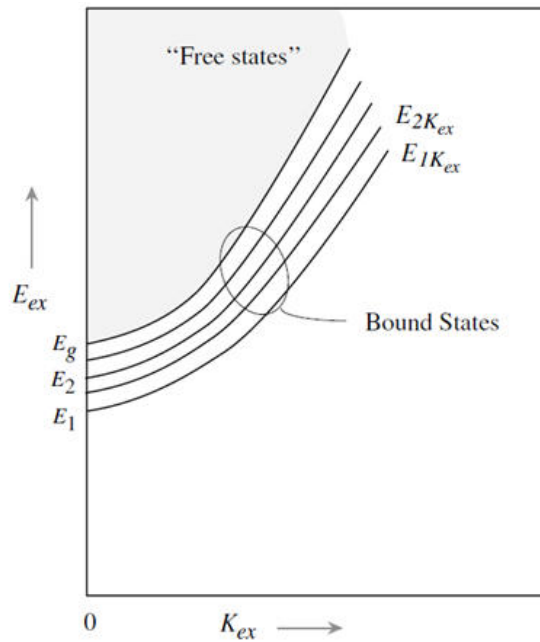


**Figure 3.46:** Sketch of the exciton band structure.

**Table 3.1:** Exciton binding energy ( $E_1$ ) and exciton radius ( $a_{ex}$ ) in direct bandgap bulk semiconductors with the zinc-blende structure (from Yu and Cardona [125]).

Semiconductor	$E_1$ (meV)	$a_{ex}$ (Å)
InP	4.9	112
GaAs	5.1	113
CdTe	11	12.2
ZnTe	13	11.5
ZnSe	19.9	10.7
ZnS	29	10.2

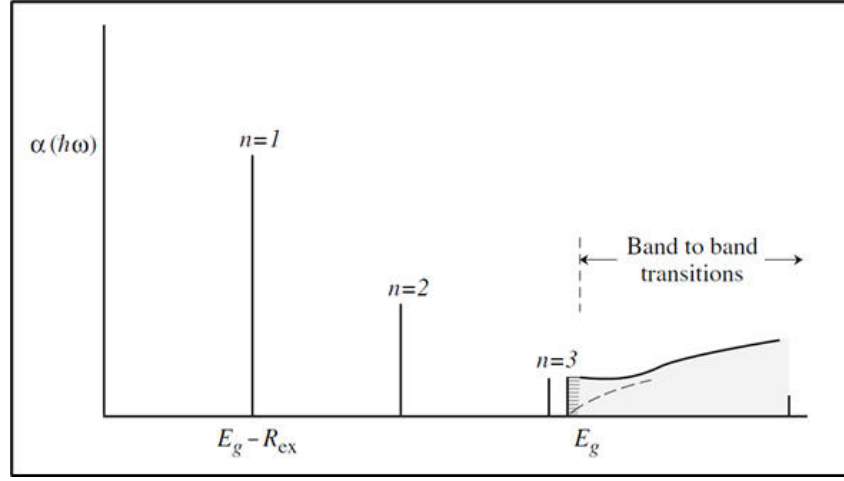


**Figure 3.47:** Schematic representation of the absorption spectrum with a few delta peaks (solid line, not on scale) in a semiconductor with excitonic effects versus photon energy. The dashed curve corresponds to the independent-electron picture (see Eq.3.12).

It can be shown (see Singh [123]) that near the band edge the absorption coefficient for optical radiation of frequency  $\omega$  can be expressed as

$$\alpha_{ex}(\omega) = \alpha_F(\omega) \frac{2\pi R_{ex}}{(\hbar\omega - E_g)^{1/2}}, \quad (3.84)$$

where  $\alpha_F(\omega)$  is the absorption coefficient without excitonic effects, i.e.,

$$\alpha_F(\omega) = C \frac{(\hbar\omega - E_g)^{1/2}}{\hbar\omega}. \quad (3.85)$$

In Eq. 3.85 the term  $(\hbar\omega - E_g)^{1/2}$  stems from the density of states corresponding to the transition from  $E_v(k)$  to  $E_c(k) = E_v(k) + \hbar\omega$  and  $C$  is a constant. By combining Eqs. 3.85 and 3.84, we see that due to the excitonic effect the absorption coefficient assumes a non-zero constant value above and down to the band edge. Below the band edge, the density of discrete excitonic bound states increases proportional to  $1/n^3$  so that the absorption coefficient may show a narrow peak with width  $\sim 1\text{meV}$  just below the band edge. Therefore, apart from a few delta peaks, corresponding to the first lowest discrete exciton bound-state levels, the absorption coefficient versus  $\hbar\omega$  assumes a non-zero value around the bandgap energy, i.e., dramatically larger than in the independent-electron picture (Eq. 3.85). This is schematically indicated in Fig. 3.47.

It should be noted that in InP and GaAs (see Table 3.1), the exciton binding energy  $R_{ex}$  is on the order of  $5\text{meV}$ , which corresponds to a thermal energy at  $\sim 57\text{K}$ . Therefore, the effects of discrete excitonic levels are visible only at temperatures far below room temperature. This is demonstrated in Fig. 3.48. Usually, at room temperature excitons don't play significant roles in bulk semiconductors. This is very different in quantum wells, where exciton effects are significantly more pronounced, as can be understood from the following considerations: When the width of the quantum well is less than the diameter of the excitonic Bohr orbit, the electron-hole separation will be limited by the quantum well width, rather than by the larger "Bohr" radius, thereby significantly increasing the Coulomb binding energy of the excitons. Thus small quantum well widths

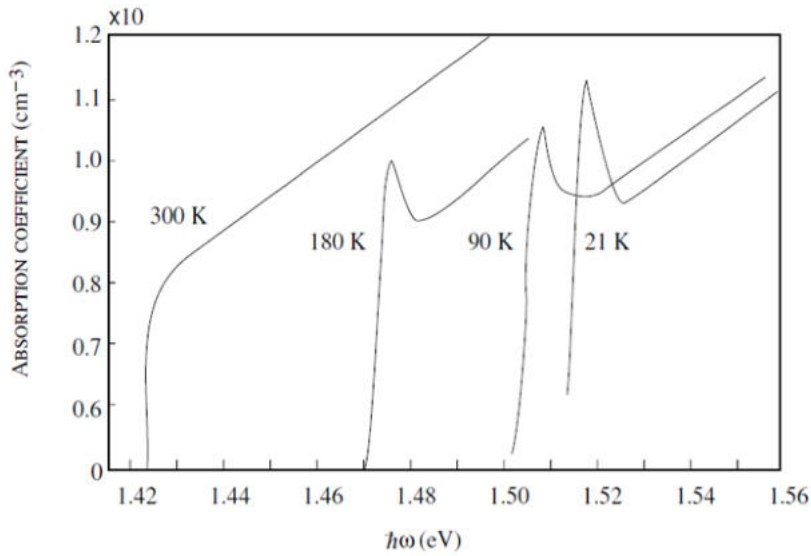


**Figure 3.48:** Typical measured absorption spectra for GaAs at various temperatures, as indicated. For each temperature, the band-to-band absorption edge corresponds to the band-gap energy at that particular temperature. Excitonic effects are no longer observable at room temperature. (From Dresselhaus[124]).

enhance exciton effects. Normally sharp exciton peaks in bulk GaAs are observed only at low temperature, but in quantum well structures excitonic effects can be observed at room temperature.

The quantum-confined Stark effect (QCSE) describes the effect of an external electric field upon the light absorption spectrum or emission spectrum of a quantum well (QW). In the absence of an external electric field, electrons and holes within the quantum well may only occupy states within a discrete set of energy sub bands. Only a discrete set of frequencies of light may be absorbed or emitted by the system. When an external electric field is applied, the electron states shift to lower energies, while the hole states shift to higher energies. This reduces the permitted light absorption or emission frequencies. Additionally, the external electric field shifts electrons and holes to opposite sides of the well, decreasing the overlap integral, which in turn reduces the recombination efficiency (i.e. fluorescence quantum yield) of the system. The spatial separation between the electrons and holes is limited by the presence of the potential barriers around the quantum well, meaning that excitons are able to exist in the system even under the influence of an electric field. The quantum-confined Stark effect is used in QCSE optical modulators, which allow optical communications signals to be switched on and off rapidly.

### 3.13 Appendix: Derivation of electron and hole density

We start with the last expression in Eq. 3.13, which can be expressed in the Boltzmann approximation as

$$n_e \cong \frac{1}{2\pi^2} \left( \frac{2m_c}{\hbar^2} \right)^{3/2} \int_{E_c}^{\infty} dE (E - E_c)^{1/2} \exp\left[-\frac{E - E_F}{k_B T}\right] \quad (3.86)$$

Note that at room temperature,  $T = 300$  K, we have  $k_B T = 0.026$  eV, whereas the energy gap in semiconductors is  $\lesssim 1$  eV. Hence, if  $E_F$  is in the energy gap and not too close to  $E_c$ , Eq. 3.86 is an excellent approximation. The integral in (3.86) can be solved by introducing

$$\eta = \frac{E - E_c}{k_B T}, \quad (3.87)$$

leading to

$$n_e \cong \frac{1}{2\pi^2} \left( \frac{2m_c k_B T}{\hbar^2} \right)^{3/2} \exp\left[-\frac{E_c - E_F}{k_B T}\right] \int_0^\infty d\eta \eta^{1/2} e^{-\eta}, \quad (3.88)$$

where the integral is tabulated and has the value  $\frac{1}{2}\sqrt{\pi}$ . Therefore, Eq. 3.88 becomes

$$n_e \cong \frac{1}{4} \left( \frac{2m_c k_B T}{\pi \hbar^2} \right)^{3/2} \exp\left[-\frac{E_c - E_F}{k_B T}\right] \quad (3.89)$$

The thermal electron concentration can thus be written as

$$n_e = N_c \exp\left[-\frac{E_c - E_F}{k_B T}\right] \quad (3.90)$$

where  $N_c$  is called the effective density of states in the conduction band,

$$N_c \cong \frac{1}{4} \left( \frac{2m_c k_B T}{\pi \hbar^2} \right)^{3/2} \quad (3.91)$$

Now we can follow a similar procedure for the holes in the valence band. Since a hole is a non-occupied electron state, the hole equilibrium distribution is not  $f_F(E)$  but rather

$$1 - f_F(E) = \frac{1}{1 + \exp\left(\frac{E_F - E}{k_B T}\right)} \approx e^{-\frac{E_F - E}{k_B T}} \quad (3.92)$$

where the last step is again the above-introduced Boltzmann approximation, valid when  $E_F - E_v \gg k_B T$  and  $E \leq E_v$ . Like Eq. 3.86 we can express the thermal-equilibrium concentration of holes in the valence band as

$$n_h \cong \frac{1}{2\pi^2} \left( \frac{2m_v}{\hbar^2} \right)^{3/2} \int_{-\infty}^{E_v} dE (E_v - E)^{1/2} \exp\left[-\frac{E_F - E}{k_B T}\right] \quad (3.93)$$

where the lower integration limit is taken as minus infinity since the exponential decays fast enough to validate this approximation. Following the same procedure as for  $n_e$  above, we now find for the thermal hole concentration

$$n_h = N_v \exp\left[-\frac{E_F - E_v}{k_B T}\right] \quad (3.94)$$

where  $N_v$  is called the effective density of states in the valence band,

$$N_v \cong \frac{1}{4} \left( \frac{2m_v k_B T}{\pi \hbar^2} \right)^{3/2} \quad (3.95)$$